9-12-2017 10:30 AM

The Onset of Convection in Rarefied Gases

Md Asif Zobaer
The University of Western Ontario

Supervisor
Dr. Roger E. Khayat
The University of Western Ontario

Graduate Program in Mechanical and Materials Engineering
A thesis submitted in partial fulfillment of the requirements for the degree in Master of Engineering Science

Abstract

The onset of convection in the Rayleigh-Bénard problem for a monatomic rarefied gas at small Knudsen number has been investigated. Compressibility-induced density variations have been considered without imposing any restriction on the magnitude of temperature difference. A linear temporal stability analysis has been conducted for a compressible slip-flow model considering a Maxwellian gas and the dispersion relation is calculated using a Chebyshev collocation method. A neutral stability curve obtained in the Froude-Knudsen number plane marks transition to convection from a pure conduction state. The critical wave number observed for the onset of convection is in good agreement with the existing literature. A comparison of two molecular interaction models: hard-sphere and Maxwellian gas, a more realistic model, for predicting the boundaries of the convection domain has been presented here which is expected to be useful for future studies on related topics using more realistic gas models.

Keywords

Rayleigh-Bénard, rarefied gas, compressibility, linear stability analysis, Chebyshev collocation method, Maxwellian gas, hard-sphere gas, neutral stability curve.

Acknowledgments

I would like to express sincerest gratitude to my supervisor Professor Roger E. Khayat for his continuous guidance and support throughout the tenure of my masters research. Without his invaluable suggestions and constant inspiration the completion of this dissertation would not have been possible. I truly appreciate his patience in understanding my difficulties while working on this project.

I would like to thank my colleagues, Mohammad Tanvir Hossain and Yunpeng Wang for their companionship, cooperation, suggestions and constant encouragement for last two years. I gratefully acknowledge the contribution of Mr. Wang in developing a MATLAB code for a part of this thesis. I am specially thankful to Dr. Christopher T. DeGroot who graciously took the time to offer his valuable insights.

Last but not the least, I thank my parents who supported me throughout my student life and my wife who has been extremely patient and supportive throughout the last two years.

Table of Contents

List of Figures

List of Appendices

Nomenclature

C_p	Specific heat at constant pressure, J/kgK
D	Gap between upper and lower plates, m
Fr	Froude number
G	Gravitational acceleration, m/s^2
k	Horizontal wave number, 1/m
K	Thermal conductivity, W/ m^2K
Kn	Knudsen number
P	Pressure, Pa
q	Heat flux, W/mK
r	Intermolecular distance, m
Ra	Rayleigh Number
s	Growth rate of the perturbation
t	Time, s
T	Temperature, K
δT	Temperature difference between upper and lower plates, K
U	Internal energy, J
v	Velocity, m/s

Greek Symbols

α	Coefficient of thermal expansion, 1/K
β_T	Compressibility, Pa^{-1}
κ	Thermal diffusivity, m^2/s
ρ	Density, kg/m^3
ϕ	Intermolecular potential, J/mol
μ	Dynamic viscosity, kg/ms
υ	Kinematic viscosity, m^2/s
ξ	Index of repulsion
χ	Accommodation coefficient

Chapter 1

1 Introduction

Thermal convection represents one of the most common forms of fluid flow. Of the two types of convection, natural convection is driven by buoyancy caused by density variation due to a temperature gradient. When an external force drives the fluid flow, it is called forced convection. In many industrial applications forced convection is important for cooling purposes such as automobile radiators, condensers, jet impingement cooling in electronic devices and so on. On the other hand, natural convection is a major feature of the dynamics of the oceans, the atmosphere, and the interior of stars and planets (Busse 1978; Getling 1998) as well as convection in the earth's mantle (Schubert, Turcotte & Olson 2001). The study of natural convection is also useful to understand the atmospheric phenomena like tornados and thunderstorms (Emanuel 1994). It is convenient to study natural convection because of its theoretical and experimental simplicity (Stranges, Khayat & Albaalbaki 2013).

1.1 Rayleigh-Bénard Convection

The most common natural convection configuration is known as Rayleigh-Bénard, shown in Figure 1.1. This configuration is defined by a thin layer of fluid confined between two plates infinite in the horizontal direction. The bottom plate is maintained at a higher temperature than the top plate. Fluid near the bottom plate becomes lighter because of thermal expansion and tries to rise due to buoyancy while denser fluid at the top plate falls, creating a bulk motion in the system. But the viscous dissipation and heat diffusion by conduction try to prevent the motion of the fluid. If the temperature difference between the plates, δT, is low enough, viscous effects keep the fluid layer motionless and a steady conduction state prevails with a linear temperature profile develops between the two plates. If the temperature difference between the plates is increased through a critical limit, the buoyancy effects overcome the retarding forces and convection sets in.

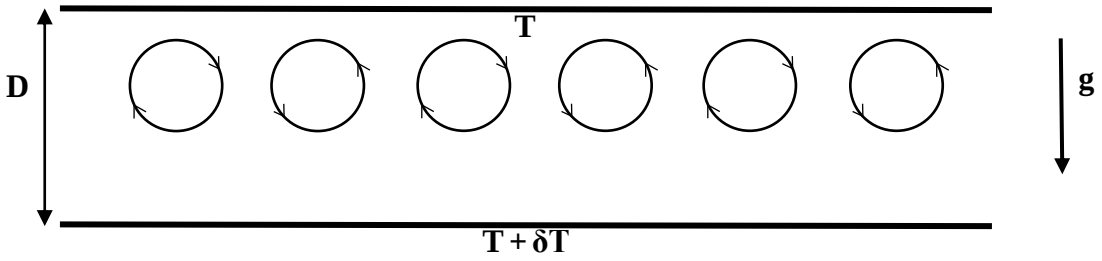

Figure 1.1: Schematic representation of Rayleigh-Bénard convection (Image reproduced from Urban et al. 2007)

The relative effects of buoyancy force, fluid viscosity, and heat conductivity is represented by a nondimensional parameter called the Rayleigh number defined as

$$\mathrm{Ra} = \frac{\delta T g \alpha D^3}{\kappa \nu}. \qquad (1.1)$$

Here g is the gravitational acceleration acting downwards, α is the coefficient of thermal expansion, D is the gap between the plates, κ is the thermal diffusivity defined as $\kappa = K/\rho C_p$ where C_p is the specific heat of the fluid, and ν is the kinematic viscosity which is the ratio of dynamic viscosity, μ and density ρ. For an incompressible fluid as considered by Lord Rayleigh (1916), convection sets in when Ra becomes larger than a critical value. The value of critical Ra depends on the choice of the boundary conditions.

1.2 Rayleigh-Bénard Convection in Incompressible Fluids

One of the most popular approaches to model the Rayleigh-Bénard convection is to apply the Boussinesq approximation. It assumes that the variation in density is solely due to the temperature difference and the density is independent of pressure. The density is hence assumed to be constant since its variation has no effect on the flow field except in the buoyancy term in a buoyancy-driven flow such as the Rayleigh-Bénard convection. The Boussinesq approximation has been widely used in studying the Rayleigh-Bénard problem which simplifies the equations governing fluid motion in order to facilitate both

theoretical and numerical computations. It provides a very good approximation to the Navier-Stokes equations for nearly incompressible fluids such as water.

Within the framework of the Boussinesq approximation, Rayleigh (1916) and Jeffreys (1926) have calculated the critical value of Ra for the onset of convection which, for the system shown in Figure 1.1, is 1708. However, their analysis neglects the effects of compressibility of the fluid.

When the temperature and associated density changes are small, the Boussinesq approximation is an excellent approximation as in the case for the ocean where the density and temperature vary by about 1% and 10% respectively between the bottom and the surface (Spiegel & Veronis 1960). It can be a reasonable approximation for the Earth's atmosphere and even in stellar interiors if the fluid layer is thinner than the local density and temperature scale heights. This approximation also provides satisfactory accuracy in modeling liquids around room temperature, natural ventilation in buildings, or dense gases dispersion in industrial set up. In a Rayleigh-Bénard configuration with a compressible fluid, the Boussinesq approximation is only valid for thin layers of fluid (Landau & Lifshitz 1959). But, compressibility effects cannot be neglected when the fluid layer is thick because the upper fluid then weighs heavily upon the lower fluid (Bormann 2001).

1.3 Rayleigh-Bénard Convection in Compressible Fluids

While the Boussinesq approximation provides a simpler way of modeling many fluid flow problems treating the fluid as incompressible, there has been an increased interest in compressible fluids, essentially stellar convection(Gauthier & Doolen 1987). The convection zones in stellar atmosphere are, in general, not thin and the Boussinesq approximation can no longer be used in such analysis (Steffen, Freytag & Ludwig 2005). The non-Boussinesq effects also need to be considered in rarefied gases commonly encountered in micro and nano-scale devices (Robinson & Chan 2004). The Boussinesq approximation is only valid when the temperature difference is small (Spiegel & Veronis 1960), but in rarefied gases instabilities are excited when the temperature differences are

large (Golshtein and Elperin 1996). . Furthermore, the Boussinesq approximation is a little precarious from a thermodynamic point of view as well. Thermodynamic stability condition derived from the second law of thermodynamics is given by

$$\alpha^2 \leq \frac{\rho c_P}{T}\beta_T \tag{1.2}$$

where β_T is the compressibility (Muller 1985). According to (1.2), β_T can only be zero if the thermal expansion coefficient is ignored. Indeed, real fluids never fully conform to the Boussinesq approximations and this departure has been studied in details by Busse (1967), Ahlers (1980) and Paolucci & Chenoweth (1987).

In the presence of compressibility, the mechanical stability of the fluid is described by the "adiabatic temperature gradient" (ATG) criterion also known as the Schwarzschild criterion (Schwarzschild & Härm 1958). According to this criterion, for a fluid particle rising through the hydrostatic pressure field the applied temperature gradient must be larger than the adiabatic temperature gradient (Landau & Lifshitz 1959),

$$\frac{\partial T}{\partial y} > \mathrm{ATG} = \left(\partial T/\partial p\right)_s \rho g \tag{1.3}$$

where subscript s denotes constant entropy. Compressibility thus brings in a source of mechanical stability (1.3) in addition to dissipative mechanism characterized by the viscosity and thermal conductivity as in the case of an incompressible fluid. Therefore, in a Rayleigh-Bénard configuration with a compressible fluid, convection does not start until the temperature difference across the layer, δT, becomes sufficiently larger than the critical value δT_R calculated from the Rayleigh condition for incompressible fluids. The compressible Rayleigh-Bénard problem was analyzed by Gitterman & Steinberg (1970). Gitterman (1978) derived an expression for the onset condition

$$\delta T_{onset} = \delta T_R + \delta T_{ad} \tag{1.4}$$

where δT_{ad} is the temperature difference from the adiabatic temperature gradient effect.

1.4 Approaches to Study the Compressible Rayleigh-Bénard Problem

Compressibility effects had been ignored in laboratory-scale experiments where it is usually too small to be observed (Kogan & Meyer 2001). But its understanding is important in many applications such as large-scale geophysical flows including earth's atmosphere and mantle convection (Tritton 1988). A popular approach to investigate the compressible Rayleigh-Bénard convection in laboratory-scale is to perform experiments under high-pressure conditions near the gas-liquid critical point. Near-critical fluids have high compressibility which has attracted great attention (Anisimov 1991). Such an approach is demonstrated in a series of papers by Ashkenazi & Steinberg (1993), Kogan & Meyer (2001), and Zappoli, Beysens & Garrabos (2015).

The other popular approach is to address the Rayleigh-Bénard problem for rarefied gases which offers the opportunity of studying different fundamental issues such as the mechanism of stability and self-organization at the molecular level and their relation to macroscopic phenomena (Cercignani 2000). Since one can investigate the microscopic origin of hydrodynamic instability with a rarefied gas system which is highly compressible, the Rayleigh-Bénard convection in rarefied gases has become a model problem.

1.5 Rayleigh-Bénard Problem in Rarefied Gas

The mechanics of rarefied gases differs from the usual gas-dynamics because the gas cannot be treated as a continuum and the effect of the random motion of each molecules must be considered. The relative importance of the microscopic molecular motion to the macroscopic mass motion of the gas is measured by a nondimensional parameter, Knudsen number which is the ratio of mean free path to the characteristics length of the system. Based on the Knudsen number, the flow regime can be classified as (Struchtrup 2005) –

1. The hydrodynamic regime: $\mathrm{Kn} \leq 0.01$
2. The slip flow regime: $0.01 \leq \mathrm{Kn} \leq 0.1$

3. The transition regime: $0.1 \leq \mathrm{Kn} \leq 10$
4. Free molecular flow: $\mathrm{Kn} \geq 10$

In the hydrodynamic regime, the flow is very well described by Navier-Stokes-Fourier (NSF) equations (Struchtrup 2005). When the Kn number is larger than 0.01, the gas becomes rarefied and fewer collision between molecules take place in the flow. The lack of collision results in significant velocity-slip and temperature-jump near the wall. As a result, NSF equations become inappropriate in the rarefied regime. Typically, to study the rarefied gas problems, the direct simulation Monte Carlo (DSMC) technique is used. The DSMC method uses a finite set of model particles denoted by their positions and velocities. A direct simulation of the molecular gas dynamics is performed over small time steps as the particles move and collide in physical space. The intermolecular collisions are modeled using stochastic rules. The proof of convergence of the DSMC algorithm to the Boltzmann equation is given by Wagner (1992). This technique was used to successfully simulate the Bénard instability for the first time by Garcia & Penland (1991) and Stefanov & Cercignani (1992).

Though the DSMC method provides detailed information about the molecular system including producing the physical fluctuations of the macroscopic quantities in a rarefied gas system, for small Kn number the onset of convection can be difficult to determine because of the presence of inherent noise (Stefanov, Roussinov & Cercignani 2002). In the slip flow regime, a popular alternative is to model the rarefied gas problem using NSF equation accompanied by proper boundary conditions that account for the velocity-slip and temperature-jump at the wall (Manela & Frankel 2005).

One of the critical physical differences between rarefied gas flow and dense gas flow is the slip in gas velocity at the solid surface. For a rarefied gas flow problems, the boundary conditions are derived from gas-solid interaction models which describe how energy and momentum are transferred to/from a surface and how reflecting molecules are scattered following a surface impact. The most popular, and simplest, model for the boundary conditions in a rarefied gas flow problem is given by Maxwell (Chapman & Cowling 1970; Cercignani 1975). The gas-surface interaction model was first developed by Maxwell (1879) that considers two kinds of interactions, the specular and diffuse

interactions. In a specularly reflecting wall, the tangential velocity of a colliding gas particle remains unchanged while the normal component of its velocity only changes sign. The gas particle and the solid molecules are assumed to be rigid elastic spheres. The particle does not exchange energy with the wall but exerts only a normal force on the wall. A diffuse interaction, on the other hand, takes place when an incident molecule attains thermal equilibrium with the solid surface and then evaporates from the surface according to the Maxwellian velocity distribution determined by the wall temperature.

However, both of the interaction models are too simple to describe realistic cases. Maxwell combined the two models together considering a fraction of particles reflected specularly after their collision with the wall while the other fraction thermalizes with the wall which he named the accommodation coefficient. The accommodation coefficient varies between zero to one depending upon the microscopic details of the wall and gas.

The velocity-slip and temperature-jump boundary conditions are also affected by the transport coefficients which in turn depend on the choice of gas model. Two gas molecules attract when they are far apart and repel each other when they come close together (Hirschfelder, Curtiss & Bird 1954). The interaction between them is expressed in terms of their intermolecular potential rather than the force acting between the molecules. The first and the simplest molecular model to be employed in the simulation of rarefied gas flows is the hard sphere model which is developed based on the rigid-sphere interaction potential. According to this model, the intermolecular potential is given by

$$\phi(r)\begin{cases} = \infty & r < r_0 \\ = 0 & r > r_0 \end{cases}$$

where r_0 is the hard sphere diameter (Hirschfelder, Curtiss & Bird 1954).

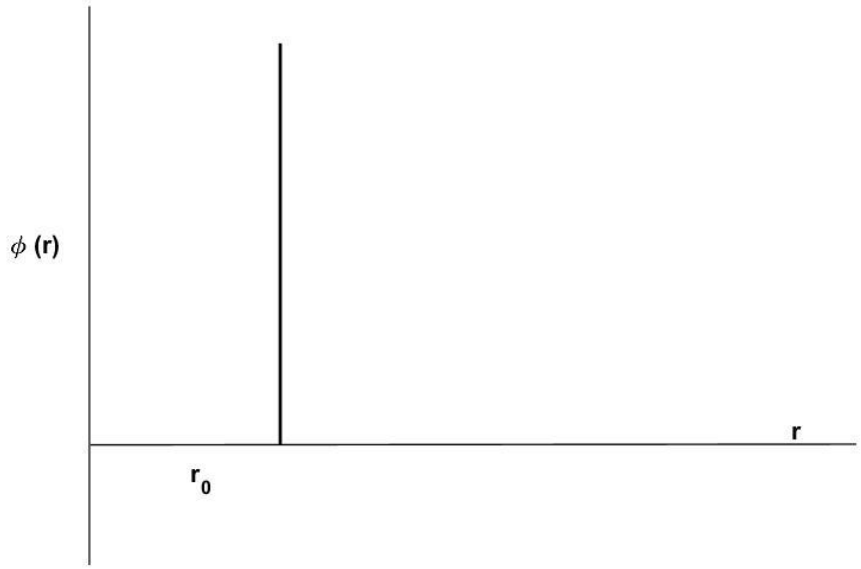

Figure 1.2: Interaction potential for hard sphere model (Image reproduced from Hirschfelder, Curtiss & Bird 1954).

Hard sphere model has been a popular gas model because of its simplicity in deriving analytical expressions for transport coefficients for rarefied gas flow problems. Stefanov et al. (1992) and Manela & Frankel (2005) worked with hard sphere model when addressing the Rayleigh-Bénard problem for rarefied gases. The hard sphere model only predicts an infinite repulsion when two gas molecules are in contact with each other (Figure. 1.2). It is the simplest model which is sufficient in some cases to account for some of the transport properties of gas accurately. However, it cannot provide any information of the repulsive force when the distance between the two molecules increases. Also, the hard sphere model does not consider the attractive forces between the molecules at large distances. One of the widely used models which accounts for both the repulsive and attractive potential is given by Lennard-Jones (Figure. 1.3).

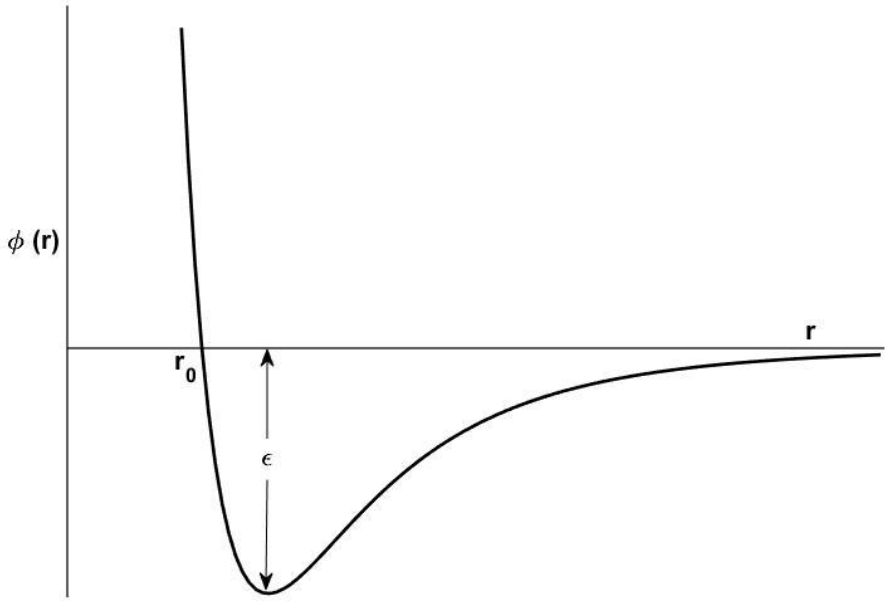

Figure 1.3: Interaction potential for Lennard-Jones model (Image reproduced from Hirschfelder et al. 1954).

The interaction potentials for repulsive forces and attractive forces are approximated using two different inverse power laws which are added together to represent the total Lennard-Jones potential and can be expressed as $\phi(r) = 4\varepsilon\left[(r_0/r)^{12} - (r_0/r)^6\right]$, where ε is the maximum energy of attraction which occurs at $r = 2^{1/6} r_0$. Though this model represents a more realistic model for interaction potential of molecules, the attractive forces can be ignored when the temperature is well above the saturation point. The potential trough ε in Figure. 1.3 is too small compared to the average kinetic energy of a collision in such a case and the interaction potential can be well represented by purely repulsive potential given by $\phi(r) = a/r^{\xi}$, where ξ is called the index of repulsion. When $\xi = 4$, the molecules are known as Maxwellian molecules (Figure. 1.4).

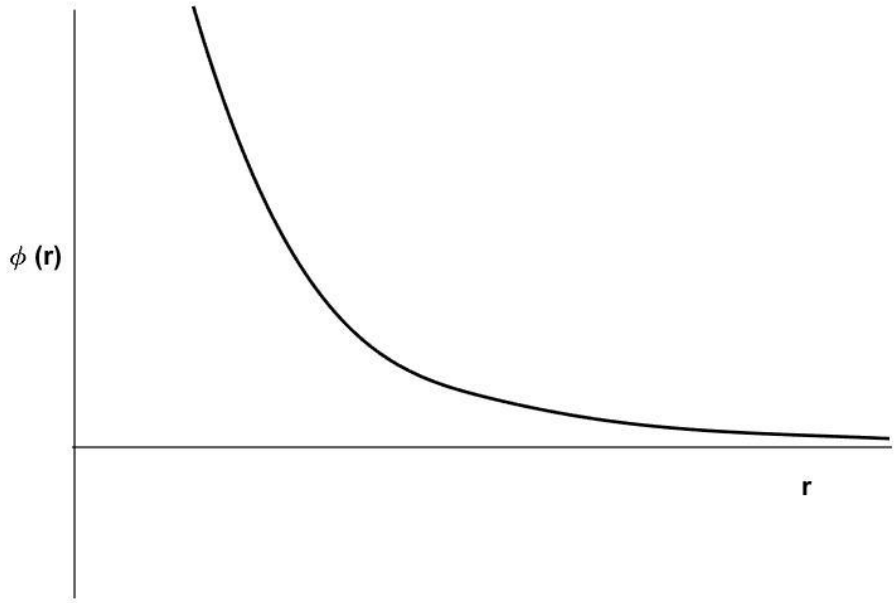

Figure 1.4: Interaction potential for Maxwellian Molecular model (Image reproduced from Hirschfelder et al. 1954).

Due to its simplicity, this model has played a fundamental role in the subsequent development of the kinetic theory. While being simple enough to express the transport coefficients analytically just like the hard sphere model, the Maxwellian molecules represent the interaction potential in the repulsive region in a more realistic way than the hard sphere model. The results obtained by Maxwell was also verified by Boltzmann (Struchtrup 2005) who repeated all the calculations using different models.

1.6 Literature Review

Rayleigh-Bénard convection is a classical problem in hydrodynamic stability theory and has been studied extensively because of its relevance to natural convection phenomena (Chandrasekhar 1961; Drazin & Reid 1981; Koschmieder 1993, Normand, Pomeau & Velarde 1977; Bergé & Dubois 1984; Bodenschatz, Pesh & Ahlers 2000). Most studies have been carried out within the framework of the Boussinesq approximation. This approximation is based on the assumptions that the temperature difference between two

plates and associated changes in density are small which are neglected everywhere except in the buoyancy term in the equation of motion. The density variation due to pressure is considered negligible and the fluid behaves as nearly incompressible. In spite of the justification for the Boussinesq approximation given in the textbook (Chandrashekhar 1961; Drazin & Reid 1981; Charru 2011) and in many literature (Spiegel & Veronis 1960; Mihaljan 1962; Hills & Roberts 1991; Rajagopal, Ruzicka & Srinivasa 1996), it has its restriction: it is only valid for a thin layer of fluid (Gray & Giorgini 1976; Frölich, Laure & Peyret 1992; Perez & Velerde 1975).

Most of the studies which have hitherto addressed the compressible Rayleigh-Bénard convection have relaxed either one of the two assumptions of the Boussinesq approximation. The effect of compressibility on the onset of convection was first acknowledged by Jeffreys 1930. Later Giterman & Shteinberg (1970), and Bormann (2001) also studied compressibility effects on the onset of convection. He obtained critical Rayleigh number based on the stability criteria formulated by Jeffreys (1930) considering the compressibility effect. However, the Rayleigh number thus obtained does not consider the effects of viscosity. On the other hand, the critical Rayleigh number accounts for the viscosity but ignores the compressibility. This led Bormann to use both the Rayleigh numbers in an additive superposition to find the true critical Rayleigh number for a compressible system. Using a linear stability analysis, he also showed that the critical Rayleigh number actually depends on the thickness of the fluid layer. However, Jeffrey (1930), Giterman & Shteinberg (1970) and Bormann (2001) considered small temperature differences which enabled them to take viscosity and thermal conductivity as constants. The effects of large temperature differences were studied by Frolich et al. (1992) but their analysis failed to account for the compressibility-induced density variations. Ahlers et al. (2010) conducted an experiment with sulfur hexafluoride at temperatures close to the gas-liquid critical point where all fluid properties vary strongly with temperature. They have found the critical temperature for the onset of convection can be significantly higher when non-Boussinesq effects are considered. But they also used very thin layers of fluid which essentially made the compressibility effects negligible. According to these studies, the onset of convection is still governed by a

critical value of Rayleigh number corresponding to a critical temperature difference greater than that of the Boussinesq case.

Unlike the two approaches to study the compressible Rayleigh-Bénard problem, Spiegel (1965) relaxed both of the assumptions of the Boussinesq approximation. Though his analysis was not restricted to small temperature differences nor to thin layers of fluid, he considered fluid viscosity and heat conductivity as constants which are not consistent with large temperature variations.

A popular approach to study the high compressible Rayleigh-Bénard problem is to conduct experiments under higher-pressure conditions near the gas-liquid critical point. Kogan & Meyer (2001) and later Furukawa et al. (2003) studied the Rayleigh-Bénard convection with Helium gas near its critical point. A similar analysis was conducted for sulfur hexa-fluoride by Roy & Steinberg (2002).

Another way to investigate the Rayleigh-Bénard problem without a *priori* restricting the temperature differences or the compressibility-induced density variation is to address the classic hydrodynamic stability problem for rarefied gases (Manela & Frankel 2005). The molecular description in a rarefied gas allows investigating the onset of convection from a kinetic viewpoint. The Rayleigh-Bénard problem for rarefied gases has become a model problem for studying fundamental issues at the molecular such as the mechanism of instability and self-organization and their relation to macroscopic phenomena (Cercignani 2000; Nicolis & Prigogine 1977; Haken 1977). The Rayleigh-Bénard convection of a rarefied gas has been numerically studied by means of the direct simulation Monte Carlo method (Watanabe, Kaburaki & Yokokawa 1994; Robinson & Harvey 1997; Golshtein & Elperin 1996; Stefanov & Cercignani 1992; Stefanov et al. 2002). Their studies showed that the transition from the pure conduction state to convection takes place for sufficiently low Kn numbers only when the temperature gradient was larger than a critical value. However, Watanabe et al. (1994) and Robinson & Harvey (1996) assumed the material properties as constants except for the density in the gravity term which allowed them to apply the Boussinesq approximation. Consequently, the transition from pure conduction to convection was determined by the nondimensional parameter, the

Rayleigh number. Golshtein & Elperin (1996) pointed out that the onset of convection could not be completely characterized in terms of a single nondimensional parameter for a rarefied gas with arbitrary temperature differences and associated compressibility effects. For a rarefied gas, the effect of gas stratification must be taken into consideration. The density of the pure conduction state, in fact, increases when moving toward the top plate which is kept at a lower temperature in the presence of weak gravity and increases when moving toward the bottom-hot plate under strong gravity. For such conditions, the authors of papers (Stefanov & Cercignani 1992; Sugimoto et al. 1995; Sone, Aoki & Sugimoto 1997) also showed that the Rayleigh number independently is insufficient to determine the stability of a rarefied gas system. Sugimoto et al. (1995) studied the effects of the Knudsen (Kn) and Froude (Fr) number, the ratio of temperatures between the two plates, and the geometry of the gas domain. They solved the Bhatnagar-Gross-Krook equation for the Rayleigh-Bénard problem using a finite-difference scheme. The zone of instability obtained from these studies established the fact that the onset of convection occurs for small Knudsen numbers only. This fact encouraged Stefanov et al. (2002) to investigate the Rayleigh-Bénard problem on the basis of a continuum model of a compressible viscous heat-conducting gas. The state-dependent transport coefficients are easily derived from the Chapman-Enskog expansion for the Boltzman equation as shown in Chapman & Cowling (1970). Stefanov et al. (2002) solved the continuum slip model for the Rayleigh-Bénard problem for a rarefied gas using a finite difference method. They also investigated the problem by a molecular based approach using the DSMC method and compared both the results for a hard-sphere gas model. For a given aspect ratio of the gas domain, Stefanov et al. (2002) obtained a neutral curve in the (Fr, Kn) plane which delineates the zones of pure conduction and convection for specific values of temperature ratios.

Numerical simulations by Stefanov et al. (2002) successfully determined the location of the neutral curve rather than merely imposing a necessary condition unlike the previous researchers. The DSMC method has been commonly used to investigate the flow and heat transfer behavior in microdevices (Bird 1194; Hadjiconstantinou et al. 2003; Vargas et al. 2014). But due to the existence of a hysteresis loop for small Kn numbers, it is difficult to clearly identify the parameters combinations in the vicinity of transition to convection

(Stefanov et al. 2002). Also, these simulations are extremely time consuming in the continuum limit (Fan & Shen 2001; Vargas et al. 2014). To avoid the difficulties associated with the DSMC techniques used by Stefanov et al. (2002), Manela & Frankel (2005) addressed the Rayleigh-Bénard problem for rarefied gases using a continuum model consisting of the Navier-Stokes equations and state-dependent transport coefficients along with velocity-slip and temperature-jump boundary conditions for monatomic hard-sphere gas. The choice of a hard-sphere gas model was inspired by Stefanov et al. (2002) who used the model because of its simplicity in the context of Monte Carlo simulation. However, unlike Stefanov et al. (2002) who used finite difference method, Manela & Frankel (2005) used the spectral method. Using the Chebyshev collocation method they transformed the system of differential equations into an algebraic eigenvalue problem to find the dispersion relation. The neutral curve Manela & Frankel (2005) obtained in the plane of (Fr, Kn) for a specific value of temperature ratio which shows remarkable agreement with that obtained by Stefanov et al. (2002). This agreement suggests the linear analysis as a useful alternative for studying the Rayleigh-Bénard problem in a rarefied gas, particularly at arbitrary small Knudsen numbers.

Since the macroscopic transport model offers reasonable accuracy along with significant computational advantages over the DSMC technique, it has been considered a suitable alternative to the Monte Carlo method (Struchtrup 2005). Higher order continuum models are derived from the Boltzmann equation based on either the Chapman-Enskog expansion (Chapman & Cowling 1970) or Grad's moment expansion method (Grad 1949). But these methods lack a complete set of boundary conditions for higher order expansion (Bobylev 2008; Bobylev & Windfall 2012). This has been overcome by regularized- 13 (R13) equations which are stable and equipped with a complete set of boundary conditions (Struchtrup & Torrilhon 2008) and are capable of providing an accurate description of rarefied gas flows (Taheri et al. 2009; Taheri, Torrilhon & Struchtrup 2009; Struchtrup & Taheri 2011; Rana, Torrilhon & Struchtrup 2013). The R13 equations has been proven computationally efficient than the DSMC method; the computational times are several orders of magnitude less than that required for highly accurate DSMC simulations (Rana, Mohammadzadeh & Struchtrup 2015).

1.7 Linear Stability Analysis

The stability of a hydrodynamic system can be determined by adding disturbances to its stationary state to see whether it retains its equilibrium state or progressively departs from the equilibrium state. The system is said to be stable if the perturbations decay gradually and is unstable if they grow with time. Stability analysis is of two types, namely, linear stability analysis and nonlinear stability analysis. In linear stability analysis, the stability of the system is examined with respect to infinitesimally small perturbations and all the terms involving second or higher order in the perturbation quantity and/or their derivatives are neglected from the governing perturbation equations. This limits the amplitude of perturbations to be very small for linear stability analysis as shown in Figure 1.5 using the "particle in a well" analogy.

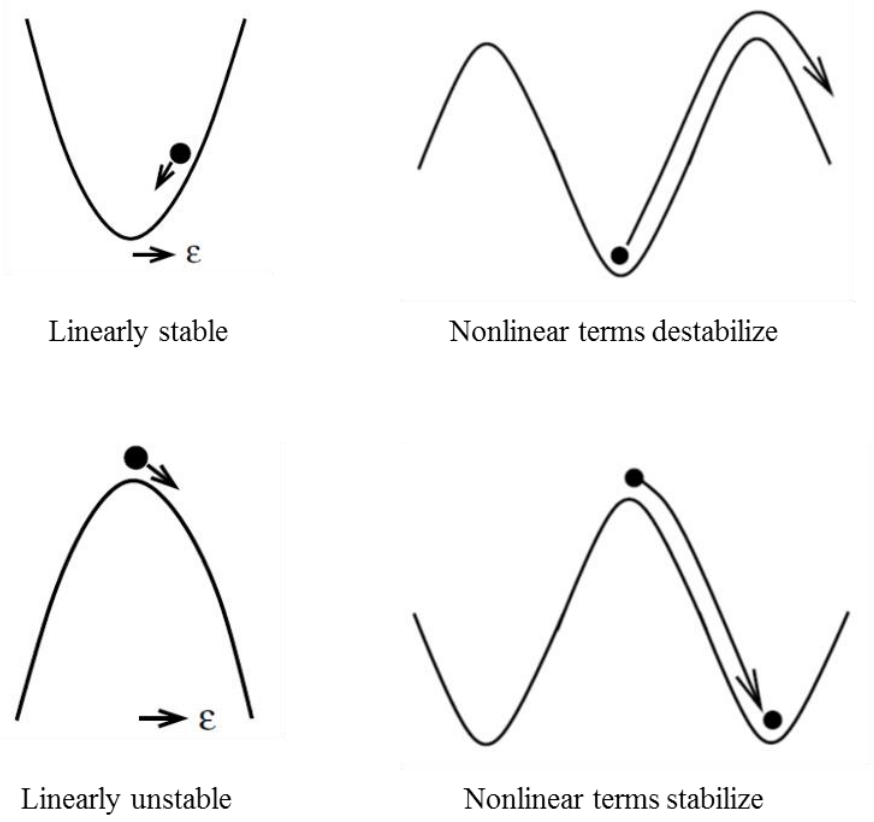

Figure 1.5: Stability of a system (Image reproduced from Fielding 2016)

A system which is linearly stable with respect to small perturbations might experience nonlinear effects that tend to destabilize it. A sufficiently large perturbation could activate the system out of the stationary state even though linear stability predicts the state to be stable. Conversely, an unstable system predicted by linear stability analysis might find a stable state when the nonlinear effects are considered. As a result, nothing can be said about the ultimate structure of the flow if the system is found to be unstable from the linear stability analysis. Yet, the linear instability analysis has been found to be useful in providing results in many stability problems which are almost in exact agreement with the experimental predictions. On the other hand, nonlinear analysis possesses the inherent difficulties involved with solving nonlinear partial differential equations.

To perform a linear stability analysis following procedure is generally followed (Drazin & Reid 1981):

1. Specifying the governing equations and boundary conditions
2. Finding the base state
3. Adding a small perturbation
4. Linearizing the equations
5. Solving the linearized equations

The application of linear stability analysis to determine the onset of convection in Rayleigh-Bénard problem for an incompressible fluid has been discussed in textbooks by Chandrasekhar (1961) and Drazin & Reid (1981). The following formulation for an incompressible fluid along with equations (1.5) – (1.19) have been adapted from Drazin & Reid (1981). Consider the liquid layer placed between two flat plates with gap D. For an incompressible fluid, the governing equations involving mass, momentum and energy conservation are simplified using the Boussinesq approximation. This approximation is based on the fact that density variations are negligible when the change in temperature is small. Also, the thermophysical properties such as coefficients of viscosity, thermal expansion, heat conductivity and specific heat capacity are considered constant. Nevertheless, density variation cannot be neglected in the buoyancy term of the Navier-Stokes equation. The density of fluid between two plates at temperature is given by

$$\rho(T)=\rho_0\left[1-\alpha(T-T_0)\right], \tag{1.5}$$

where ρ_0 is the density of the fluid at bottom-plate temperature, T_0 and α is the coefficient of thermal expansion. Typically the value of α is of order 10^{-3} for gases and 10^{-4} for liquids. Density variation can be neglected when working with small temperature change since $(\rho-\rho_0)/\rho_0=\alpha(T_0-T)\ll 1$. But when multiplied by gravity, its effect can no longer be ignored.

We let $T_b(y)$ and $p_b(y)$ be the (base) temperature and pressure that correspond to steady state conduction. There are no base velocity. To nondimensionalize the perturbation equations, we use D for length scale, D^2/κ for time scale and κ/D for velocity scale. We also let $\theta=(T-T_b)/\beta D$ and $p=D^2(P-p_b)/\rho_0\kappa^2$ be the deviation for the temperature and pressure from the base values.

where $\beta=(T_0-T_1)/D$ is the thermal gradient at the base state. Here κ is the thermal diffusivity defined as $\kappa=k/\rho_0 c$, where k is the thermal conductivity and c is the specific heat capacity of the fluid.

The linearized non-dimensional perturbation equations finally become (asterisk to denote the dimensionless parameters has been omitted)

$$\frac{\partial u}{\partial x}+\frac{\partial v}{\partial y}=0, \tag{1.6}$$

$$\left.\begin{aligned}\frac{\partial u}{\partial t}&=-\frac{\partial p}{\partial x}+\mathrm{Pr}\left(\frac{\partial^2 u}{\partial x^2}+\frac{\partial^2 u}{\partial y^2}\right),\\ \frac{\partial v}{\partial t}&=-\frac{\partial p}{\partial y}+\mathrm{Ra}\,\mathrm{Pr}\,\theta+\mathrm{Pr}\left(\frac{\partial^2 v}{\partial x^2}+\frac{\partial^2 v}{\partial y^2}\right),\end{aligned}\right\} \tag{1.7}$$

$$\frac{\partial \theta}{\partial t}-v=\frac{\partial^2\theta}{\partial x^2}+\frac{\partial^2\theta}{\partial y^2}, \tag{1.8}$$

where Ra is the Rayleigh number given by $Ra = g\alpha\beta d^4 / \kappa\upsilon$ and the Prandtl number by $Pr = \upsilon / \kappa$ and υ being the kinematic viscosity.

It is possible to eliminate all the dependent variables and obtain a single stability equation involving the vertical velocity of the perturbation, v:

$$\left(\frac{\partial}{\partial t} - \Delta\right)\left(\frac{1}{Pr}\frac{\partial}{\partial t} - \Delta\right)\Delta v = Ra\frac{\partial^2 v}{\partial x^2}, \tag{1.10}$$

where Δ is the Laplacian operator given by $\Delta = \partial^2/\partial x^2 + \partial^2/\partial y^2$.

The boundary conditions can either be no-slip or free surface at both or one of the plates. For illustration purposes, free-free boundary conditions have been used. Free-free boundary condition implies that normal velocity as well as shear stress at the surface are zero:

$$v(x, y = 0, t) = v(x, y = 1, t) = 0, \tag{1.11}$$

$$\frac{\partial u}{\partial y}(x, y = 0, t) = \frac{\partial u}{\partial y}(x, y = 1, t) = 0, \tag{1.12}$$

The temperature of the fluid at the boundary is same as the plate, hence

$$\theta(x, y = 0, t) = \theta(x, y = 1, t) = 0. \tag{1.14}$$

Also, using the continuity equation (1.6) we get

$$\frac{\partial^2 v}{\partial y^2}(x, y = 0, t) = \frac{\partial^2 v}{\partial y^2}(x, y = 1, t) = 0. \tag{1.13}$$

Since the linearized governing equations and the boundary conditions are symmetric in x, normal mode of the form

$$v = \bar{v}(y)e^{st+ikx} \text{ and } \theta = \bar{\theta}(y)e^{st+ikx} \tag{1.15}$$

can be taken for the perturbations. Here $s = \sigma + i\omega$ is the growth rate of the perturbation and k is the horizontal wave number. The equations then become an eigenvalue problem of the form

$$\left(D^2 - k^2\right)\left(D^2 - k^2 - s\right)\left(D^2 - k^2 - s/Pr\right)\bar{v} = -k^2 Ra\bar{v} \tag{1.16}$$

along with the boundary conditions

$$\bar{v} = D^2\bar{v} = D^4\bar{v} = 0 \text{ at y=0, 1.} \tag{1.17}$$

The solution is the complete set of eigenfunctions given by

$$\bar{v} = \sin \pi z \tag{1.18}$$

where the eigenvalue relation is

$$\left(\pi^2 + k^2\right)\left(\pi^2 + k^2 + s\right)\left(\pi^2 + k^2 + s/\mathrm{Pr}\right) = k^2 \mathrm{Ra}\,. \tag{1.19}$$

For marginal stability, s must be zero and the critical Ra number for the onset of convection is given by (Chandrashekhar 1961)

$$\mathrm{Ra}\left(k\right) = \frac{\left(k^2 + \pi^2\right)^3}{k^2} \tag{1.20}$$

In reality, the number of waves in a unit length cannot be imposed on the system. However, we can plot the values of Ra for different k for the onset of convection to see the wavelength of the disturbances that we anticipate at a particular Ra number. Figure 1.6 shows the curve (1.5) for different k (curve A). The minimum value of Ra for free-free boundary conditions is 657.5 and the corresponding wavenumber $k \approx 2.2$. When Ra is just a little greater than the minimum values, thermal instability ensues with horizontal wavelength of $2\pi d / 2.2 = 2.83d$.

For no-slip boundary conditions, the minimum value of Ra is 1708 which corresponds to the wavenumber 3.1 (Figure 1.6).

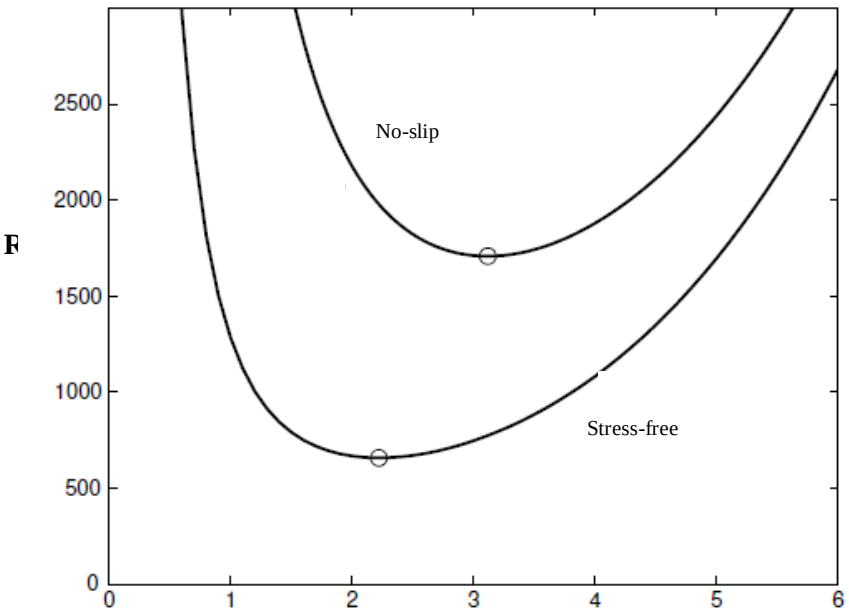

Figure 1.6: Marginal stability curves of a Rayleigh-Bénard system for two boundary conditions (Image reproduced from Mutabazi, Wesfreid & Guyon 2006)

1.8 Spectral Method

In contrast to traditional methods like finite-element and finite-difference methods for solving differential equations, spectral methods can achieve a higher degree of accuracy. In spectral methods, a trial function is used to provide the approximate representation of the solution. The trial functions are basically linear combinations of suitable basis functions. The choice of basis functions in spectral methods distinguishes them from the other numerical approaches such as finite element and finite difference methods. Spectral methods use basis functions which are smooth and nonzero over the whole domain. In finite element method, basis functions are only nonzero in the subdomains. In practice, finite-element methods are particularly well suited to problems involving complex geometry, but spectral methods can provide superior accuracy when the computational domain is rather simple.

The trial functions most commonly used are trigonometric functions or orthogonal polynomials. If the function under consideration is periodic, Fourier series approximation is used, but its convergence is not uniform near the boundaries when the function is not periodic because of the existence of Gibbs phenomenon at the boundaries. For non-periodic problems, orthogonal polynomials like Chebyshev polynomials or Legendre polynomials are advisable. Since the Chebyshev polynomials can be written in terms of a cosine Fourier series, fast Fourier transform is possible with Chebyshev series expansion which provides a faster convergence. However, fast transform algorithm is not available in the Legendre polynomials.

Along with the trial function, a suitable test function, also known as the weighting function, is applied so that the differential equation and the boundary conditions are satisfied as closely as possible by the truncated series expansion. Since the truncated expansion produces an error or residual, it is necessary to minimize the residual which is known as the method of weighted residuals. This also requires the residual to satisfy a suitable orthogonality condition with respect to the chosen test function.

The choice of the test functions distinguishes between the three basic types of spectral schemes, namely, the Galerkin, tau, and collocation methods. In collocation method, the test functions are the translated Dirac delta functions centered at some fixed points known as the collocation points.

In Chebyshev-collocation method, the trial function is approximated by a Chebyshev polynomial which satisfies the governing equation at the chosen collocation points. Unlike the equally spaced collocation points in a Fourier series approximation, the collocation points for a Chebyshev polynomials are defined by Gauss-Lobatto points,

$$x_i = \cos\frac{\pi i}{k}, \qquad i = 0, \ldots, k. \tag{1.6}$$

Other sets of points can also be used as collocation points as shown by Canuto et al. (2006) and Gottlieb, Hussaini & Orszag (1984). For example, Gauss points are useful when the boundary points $x = \pm 1$ are not included in the set of collocation points. The

Gauss-Radau points are used when the boundary point $x = -1$ needs to be excluded as in the case of cylindrical coordinates where $x = -1$ corresponds to the axis. However, for the solution of the boundary value problem considered in this thesis, Gauss-Lobatto points must be used.

The Chebyshev polynomial of degree k is defined for $x \in [-1,1]$ is given by

$$T_k(x) = \cos\left(k \cos^{-1} x\right), \qquad k = 0,1,2... \tag{1.7}$$

which reaches its extremal values ± 1 at the collocation points (intro 1).

The Chebyshev approximation of a function $u(x)$ is given by the trial function $u_N(x)$ defined for $x \in [-1,1]$:

$$u_N(x) = \sum_{k=0}^{N} \hat{u}_k T_k(x). \tag{1.8}$$

The coefficients of the approximating expansion $\hat{u}_k$, $k = 0,....,N$, is found by setting the residual function zero at the collocation points. It is, however, possible to consider, as unknowns, either the coefficients of the expansion or the values of the approximating function itself, $u_N(x_i)$ at the collocation points. The later approach is more commonly is used in the problems of fluid mechanics.

To fully transform the differential equation into algebraic equations involving the grid values $u_N(x_i)$ at the collocation points, the derivatives are also expressed in terms of $u_N(x_i)$, for a *p*th order derivative:

$$u_N^{(p)}(x_i) = \sum_{j=0}^{N} d_{i,j}^{(p)} u_N(x_j), \qquad i = 0,....,N\ . \tag{1.9}$$

The numerical values of the differentiation coefficients $d_{i,j}^{(p)}$ depend on the number of the collocation points (Peyret, 2002).

An example of how a system of differential equation can be transformed into a set of algebraic equations using the Chebyshev-collocation method is illustrated in Appendix 1.

1.9 Motivation

Understanding of heat transfer in microscales is important for performance enhancement of micro electromechanical systems (MEMS) (Beskok 2001). MEMS refer to devices which have a characteristic length of less than 1 mm and can be as small as a few microns (Stone, Stroock & Ajdari 2004; Duan & Muzychka 2007; Ghiaasiaan 2011). Most microelectromechanical system (MEMS) devices need to be packaged in vacuum before usage in order to obtain a stable performance (Liu et al. 2007; Yang, Wu & Fang 2005). Typically, such a package consists of a hot chip on one plate and several other plates maintained at a lower temperature. The gas inside the closed package transfers heat from the hot plate to the cold plates. Because of the size of the MEMS devices, the mean free path of the gas becomes comparable to the characteristic length of the device and the gas inside such devices are usually rarefied (Liu et al. 2007).

The rarefied gas flow problems has been studied previously by the DSMC method which is very expensive in computational time. The alternative to this is to investigate the problem from a continuum approach derived from the expansion of the Boltzmann equation. The R13 equations provide the most accurate description of rarefied gas flow which has only been well established for Maxwell molecules for linear as well as nonlinear cases. However, the onset of convection in a Rayleigh-Bénard problem has only been addressed for hard-sphere molecules both with the DSMC technique and the continuum approach for Navier-Stokes-Fourier (NSF) equations which is the first order expansion of the Boltzmann equation. Since the Maxwell molecules represent a more realistic interaction between the gas molecule than the hard-sphere model, studying the Rayleigh-Bénard problem for a Maxwellian molecular model with the NSF equations would not only provide a clearer information on the onset of convection in such a system

but would also create the bridge so that higher order R13 equations can be employed to the classic stability problem.

1.10 Objective

The main objective of this thesis is to investigate the onset of thermal convection in a Rayeligh-Bénard configuration for rarefied gases. To avoid the difficulties in DSMC technique, the rarefied gas problem will be approached by a continuum slip model consisting of the Navier-Stokes equation along with the first-order velocity slip and temperature-jump conditions and the transport coefficients for a monatomic Maxwellian gas. The effects of gas rarefaction, slip, and gas stratification on the pure conduction state will be analyzed. The stability of the pure conduction studied via linear stability analysis to obtain the neutral curve marking transition to convection in the Froude-Knudsen plane. The results will also be compared with those obtained for a hard-sphere gas.

1.11 Outline of the Dissertation

The dissertation is divided into four chapters: Introduction, Steady Pure Conduction State, Linear Stability Analysis, and Conclusion.

Chapter 2 analyzes the pure conduction state in a Rayleigh-Bénard configuration with a rarefied gas. The formulation of the governing equations consisting of the Navier-Stokes-Fourier equations and the development of the boundary conditions according to Maxwell's model is discussed. The motionless steady base state is explored for different combinations of parameters. A comparison between the pure conduction states for two different gas models, Maxwell and hard-sphere is presented at the end of the chapter.

The third chapter investigates the stability of the pure conduction state explored in Chapter 2 via linear stability analysis which shows that a neutral curve in the Froude-Knudsen plane delineates the zone of convection. The conditions for the onset of convection in a rarefied gas which is different than the onset condition for incompressible fluids is discussed in this chapter. Chapter 3 also analyzes the differences in the neutral curves obtained for a Maxwellian gas and that for a hard-sphere gas.

The last chapter provides a brief summary of the present work and discusses some its limitations. The scopes of further study on the Rayleigh-Benard convection are explored and some recommendations for future researches are also pointed out in Chapter 4.

Chapter 2

2 The Base State

The Rayleigh-Bénard configuration consists of a horizontal layer of fluid with its lower side hotter than the upper side. As temperature gradient develops across the layer which creates a density variation, an upward flow driven by buoyancy may start in the fluid. If the temperature gradient is not large enough, no flow is initiated due to the stabilizing effects of viscosity, thermal diffusivity, and compressibility. Due to thermal diffusion, heat is diffused through the gas which results in a lower temperature gradient across the fluid layer. When the compressibility effects are considered, density variation is no longer due to the temperature difference only and the density of the fluid may actually be larger at the bottom even with a higher temperature there as the fluid at the top weighs heavily down on the fluids near the bottom plate (Golshtein & Elperin 1996; Stefanov et al. 2002; Manela & Frankel 2005). In the absence of fluid flow, heat is transferred from the lower surface to the upper one through conduction only. Under such conditions the system is said to be in a pure conduction state. Before discussing the pure conduction state, a general formulation of the Rayleigh-Bénard problem for rarefied gases are developed in the next section.

2.1 Problem Formulation

A layer of a rarefied gas is assumed to be confined between two horizontal walls kept at a distance D. The lower and upper walls are maintained at temperatures of T_h and T_c, respectively, where $T_h > T_c$. The fluid layer is assumed to be of infinite horizontal extent. The problem is governed by the conservation of mass, linear momentum and energy equations written in Cartesian system of coordinates (x, y) whose origin lies on the lower wall with y axis pointing upwards (opposite to the direction of g, the gravitational acceleration):

$$\frac{\partial \rho}{\partial t} + \frac{\partial (\rho v_k)}{\partial x_k} = 0, \tag{2.1}$$

$$\rho \frac{Dv_i}{Dt} = -\frac{\partial p}{\partial x_i} - \rho g \delta_{iy} + \frac{\partial \sigma_{ik}}{\partial x_k}, \tag{2.2}$$

$$\rho \frac{Du}{Dt} = -\frac{\partial q_k}{\partial x_k} - \left(p\delta_{kl} + \sigma_{kl}\right)\frac{\partial v_k}{\partial x_l}, \tag{2.3}$$

along with the equations of state for an ideal monatomic gas:

$$p = \rho\theta \ , \tag{2.4}$$

$$\text{and, } u = \frac{3}{2}\theta. \tag{2.5}$$

In the above equations, summation of repeated index is implied, D/Dt denotes the material derivative and δ_{ij} is the Kroncker delta. Here t is the time and x_k are position coordinates, while ρ, v_k, p, σ_{ik}, u, and q_k denote the mass density, velocity, pressure, stress tensor, internal energy density, and heat flux. Here, θ represents the temperature in energy units defined as $\theta = RT$, where R is the gas constant and T is the thermodynamic temperature. The heat flux vector and stress tensor in (2.2) and (2.3) are defined through Fourier's law for heat conduction and Newton's law of viscosity, namely

$$q_i = -k\frac{\partial \theta}{\partial x_i}, \tag{2.6}$$

$$\sigma_{ij} = -2\mu\left[\frac{1}{2}\left(\frac{\partial v_i}{\partial x_j} + \frac{\partial v_j}{\partial x_i}\right) - \frac{1}{3}\delta_{ij}\frac{\partial v_k}{\partial x_k}\right] \tag{2.7}$$

where k is the thermal conductivity and μ denotes dynamic viscosity which can be calculated with the formulas derived using the kinetic theory of gases. Since both of the coefficients depend on temperature, a relation between them can be established making use of the dimensionless parameter Prandtl number, Pr, which is defined as the ratio of momentum diffusivity to thermal diffusivity. The measured values for all monatomic

gases are very close to $2/3$. Thermal conductivity and viscosity is thus related by the following relation (Struchtrup 2005)

$$k = (15/4)\mu. \tag{2.8}$$

In the continuum regime, the gas flow problem is specified by the boundary conditions which state that there is no relative normal or tangential velocity between the gas and the solid surface and the layer of gas is in thermal equilibrium condition at the solid-gas interface. In the slip region, there is significant nonequilibrium because of the molecular nature of the gas and the boundary conditions need to be modified (Ghiaasiaan 2011). While the condition of zero relative normal velocity still holds in the slip flow regime, the relative tangential or slip velocity is no longer zero but is a definite function of the velocity, temperature, and pressure gradients of the gas layer immediately adjacent to the wall (Sochi 2011; Shu, Teo & Chan 2017). Similarly, the gas temperature also differs from the wall temperature by a finite amount, referred to as the temperature jump (Shu et al. 2017).

Figure 2.1 shows the velocity and temperature condition at a gas-solid interface. The solid boundary moves with a velocity V_w in the tangential direction and the temperature of the solid boundary is T_w. The two plots on the left (Figure 2.1) shows the no slip condition while the plots on the right depict a slip in the velocity and a jump in the temperature of the gas. Under the slip boundary conditions, the velocity and temperature of the gas are given by V_g and T_g, respectively. Here, velocity slip is given by $V_g - V_w$ and the temperature-jump is $T_g - T_w$.

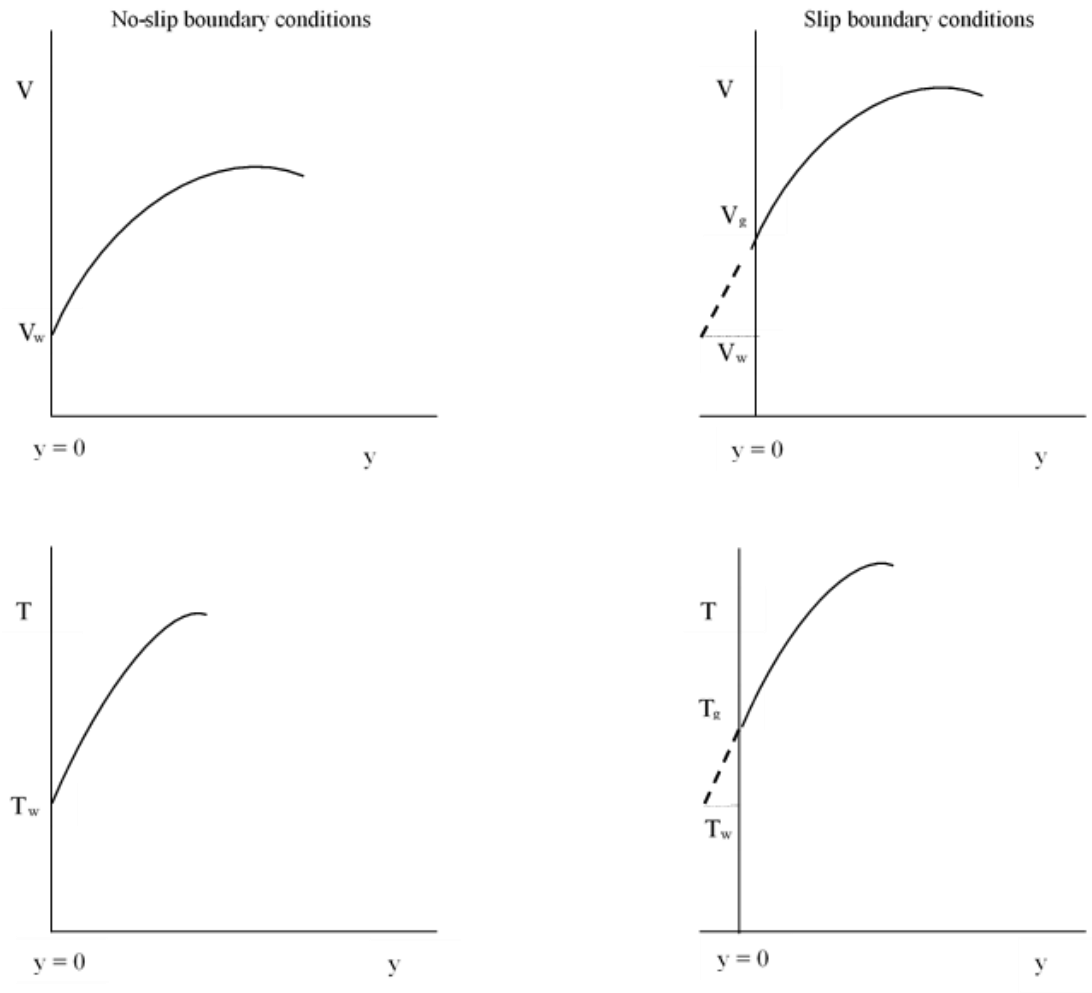

Figure 2.1: The velocity and temperature conditions at a gas–solid interface (Image reproduced from Ghiaasiaan 2011)

It has been found by many researchers including Schaaf and Chambré (1961), Deissler (1964), Beskok, Karniadakis & Trimmer (1996), Struchtrup & Weiss (2000), along with von Smouluchowski's experimental results (Kennard 1938) that the slip velocity and temperature jump are proportional to the velocity gradient and the temperature gradient normal to the wall which exists in the gas at the vicinity of the wall. The interaction between the gas molecules and solid walls which is manifested in the velocity slip and temperature jump have been expressed using Maxwell's single accommodation coefficient because of its simplicity and due to the fact that the other best-known model

does not consider the thermal slip which limits its reliability (Pan et al. 2002; Shu et al. 2017).

According to Maxwell's model, a certain fraction χ of incident gas molecules are absorbed by the wall and are then reemitted diffusely in all directions, whereas the remaining $1-\chi$ molecules reflect elastically from the wall like light rays from a plane mirror. Here χ is called the accommodation coefficient. The boundary condition for slip velocity at the wall is derived by relating the distribution of incident particles to that of the reflected ones using the Maxwellian distribution function. The velocity slip and temperature jump are thus given by (Struchtrup 2005)

$$u = -\frac{2-\chi}{\chi}\sqrt{\frac{\pi}{2}}\frac{1}{\rho\sqrt{\theta}}\sigma_{xy} \tag{2.9}$$

$$\text{and } \theta - \theta_W = -\frac{2-\chi}{\chi}\sqrt{\frac{\pi}{2}}\frac{1}{2\rho\sqrt{\theta}}q_y \tag{2.10}$$

where u and v denote the tangential and normal component of velocity along x and y axes respectively and θ_W is the local temperature at the wall.

So the boundary conditions at bottom and top walls read, including the no penetration condition along with the velocity slip and temperature jump (Struchtrup 2005), as

$$\left.\begin{aligned} v &= 0, \\ \sigma_{xy} &= -\frac{\chi}{2-\chi}\sqrt{\frac{2}{\pi\theta}}pu, \\ q_y &= -\frac{\chi}{2-\chi}\sqrt{\frac{2}{\pi\theta}}2p\left(\theta-\theta_W\right) \end{aligned}\right\} \tag{2.11}$$

at the lower wall, y = 0 and

$$\left.\begin{aligned} v &= 0, \\ \sigma_{xy} &= \frac{\chi}{2-\chi}\sqrt{\frac{2}{\pi\theta}}pu, \\ q_y &= \frac{\chi}{2-\chi}\sqrt{\frac{2}{\pi\theta}}2p\left(\theta-\theta_W\right) \end{aligned}\right\} \tag{2.12}$$

at the upper wall, y = D.

Standard normalization in studies of the Rayleigh Bénard (RB) problem in rarefied gases is used to nondimensionalize the problem. Dimensionless variables are obtained through dividing the variables by their respective reference values such as $x^* = x/D$ where D is the reference length and the superscript * is used to denote the dimensionless variable. For simplicity, the superscript * is discarded in later expressions. The reference time, velocity, density, temperature, stress and heat flux are, respectively, taken as $D/V_h, V_h, \rho_h, T_h, \mu_h V_h/D$ and $\mu_h\theta_h/D$ where V_h is the thermal speed defined as $V_h = \sqrt{RT_h} = \sqrt{\theta_h}$ (Stefanov et al. 2002; Manela & Frankel 2005) and $\theta_h = RT_h$ is the temperature in energy units evaluated at the lower (hot) wall temperature, T_h. Here ρ_h and μ_h denote values of density, and stress at temperature T_h.

Thus, in dimensionless form the governing equations become:

$$\frac{\partial\rho}{\partial t} + \frac{\partial(\rho u)}{\partial x} + \frac{\partial(\rho v)}{\partial y} = 0, \tag{2.13}$$

$$\begin{aligned} \rho\left(\frac{\partial u}{\partial t} + u\frac{\partial u}{\partial x} + v\frac{\partial u}{\partial y}\right) = & \\ & -\frac{\partial p}{\partial x} - Kn\left[-\frac{4}{3}\theta\frac{\partial^2 u}{\partial x^2} - \theta\frac{\partial^2 u}{\partial y^2} - \frac{1}{3}\theta\frac{\partial^2 v}{\partial x\partial y}\right] \\ & -Kn\left[-\frac{4}{3}\frac{\partial\theta}{\partial x}\frac{\partial u}{\partial x} - \frac{\partial\theta}{\partial y}\frac{\partial u}{\partial y} - \frac{2}{3}\frac{\partial\theta}{\partial x}\frac{\partial v}{\partial y} - \frac{\partial\theta}{\partial y}\frac{\partial v}{\partial x}\right], \end{aligned} \tag{2.14}$$

$$\rho\left(\frac{\partial v}{\partial t}+u\frac{\partial v}{\partial x}+v\frac{\partial v}{\partial y}\right)=$$

$$-\frac{\partial p}{\partial y}-Kn\left[-\theta\frac{\partial^2 v}{\partial x^2}-\frac{4}{3}\theta\frac{\partial^2 v}{\partial y^2}-\frac{1}{3}\theta\frac{\partial^2 u}{\partial x\partial y}\right]$$

$$-Kn\left[-\frac{\partial\theta}{\partial x}\frac{\partial v}{\partial x}-\frac{4}{3}\frac{\partial\theta}{\partial y}\frac{\partial v}{\partial y}-\frac{\partial\theta}{\partial x}\frac{\partial u}{\partial y}+\frac{2}{3}\frac{\partial\theta}{\partial y}\frac{\partial u}{\partial x}\right]-\frac{1}{Fr}\rho, \qquad (2.15)$$

$$\frac{3}{2}\rho\left(\frac{\partial\theta}{\partial t}+u\frac{\partial\theta}{\partial x}+v\frac{\partial\theta}{\partial y}\right)=$$

$$\frac{15}{4}Kn\left[\theta\frac{\partial^2\theta}{\partial x^2}+\left(\frac{\partial\theta}{\partial x}\right)^2\right]+\frac{15}{4}Kn\left[\theta\frac{\partial^2\theta}{\partial y^2}+\left(\frac{\partial\theta}{\partial y}\right)^2\right]-p\left(\frac{\partial u}{\partial x}+\frac{\partial v}{\partial y}\right)$$

$$-Kn\theta\left(-\frac{4}{3}\frac{\partial u}{\partial x}\frac{\partial u}{\partial x}-\frac{4}{3}\frac{\partial v}{\partial y}\frac{\partial v}{\partial y}-2\frac{\partial u}{\partial y}\frac{\partial u}{\partial y}-2\frac{\partial v}{\partial x}\frac{\partial v}{\partial x}-4\frac{\partial u}{\partial y}\frac{\partial v}{\partial x}+\frac{4}{3}\frac{\partial u}{\partial x}\frac{\partial v}{\partial y}\right), \qquad (2.16)$$

and $p=\rho\theta$. (2.17)

The dimensionless parameters appearing in the equations are the Knudsen number, representing the ratio of λ, the mean free path and gap between two walls, D, is defined as $Kn=\mu_h/\rho_h\sqrt{\theta_h}D$. The Froude number, $Fr=V_h^2/gD$ describes the relative magnitudes of gas inertia and gravity.

The governing equations are supplemented by the normalization condition derived from the conservation of mass

$$\int_0^1\rho dy=1, \qquad (2.18)$$

which represents mass flowing through a unit volume specifying the total amount of gas between the walls, and by the boundary conditions written in terms of dimensionless variables:

$$\left.\begin{aligned} &v = 0, \\ &Kn\left[\theta\left(\frac{\partial u}{\partial y}\right)\right] = -\frac{\chi}{2-\chi}\sqrt{\frac{2}{\pi\theta}}pu, \\ &Kn\left[\frac{15}{4}\theta\frac{\partial\theta}{\partial y}\right] = -\frac{\chi}{2-\chi}\sqrt{\frac{2}{\pi\theta}}2p\left(\theta-\theta_W\right) \end{aligned}\right\} \quad \text{at } y = 0 \tag{2.19}$$

and

$$\left.\begin{aligned} &v = 0, \\ &Kn\left[\theta\left(\frac{\partial u}{\partial y}\right)\right] = \frac{\chi}{2-\chi}\sqrt{\frac{2}{\pi\theta}}pu, \\ &Kn\left[\frac{15}{4}\theta\frac{\partial\theta}{\partial y}\right] = \frac{\chi}{2-\chi}\sqrt{\frac{2}{\pi\theta}}2p\left(\theta-\theta_W\right) \end{aligned}\right\} \quad \text{at } y = 1. \tag{2.20}$$

2.2 Pure Conduction State

The pure conduction state, when the velocity components are zero $\left(u = v = 0\right)$, is governed by the linear momentum equation and energy equation in y-direction given in (2.15) and (2.16) which translates to

$$\frac{d(\rho\theta)}{dy} + \frac{\rho}{Fr} = 0 \text{ and} \tag{2.21}$$

$$\theta\frac{d^2\theta}{dy^2} + \left(\frac{d\theta}{dy}\right)^2 = 0 \tag{2.22}$$

the temperature jump boundary conditions (2.19 & 2.20) read:

$$Knq_y = -\frac{2\chi}{2-\chi}\sqrt{\frac{2}{\pi\theta}}p\left(\theta-\theta_W\right) \text{ at } y = 0 \tag{2.25}$$

and $\mathrm{Knq}_y = \frac{2\chi}{2-\chi}\sqrt{\frac{2}{\pi\theta}}p\left(\theta-\theta_W\right)$ at y =1. (2.26)

System 2.21 – 2.22, together with the boundary conditions 2.25 – 2.26 needs to be solved numerically.

2.3 Numerical Solution and Validation

The solution method uses variable step-size, finite difference discretization based on the Simpson method with deferred corrections (Kierzenka & Shampine 2001, 2008). The resulting algebraic system has been solved using a simplified Newton (chord) method with residual control. Selection of the number and distribution of grid points is done automatically to meet the specified error bounds. The value of the residual set at 10^{-6} was found to be sufficient in most of the computation. Some of the critical points were tested with error bounds 10^{-10} and no significant changes in temperature and density field were observed.

In order to check on the accuracy of the numerical technique employed for the solution of the problem considered, it is validated with Stefanov et al. (2002) for the temperature and density profiles, which are depicted in Figure 2.2 and 2.3. Both results are well matched and this provides confidence in the accuracy of the present work.

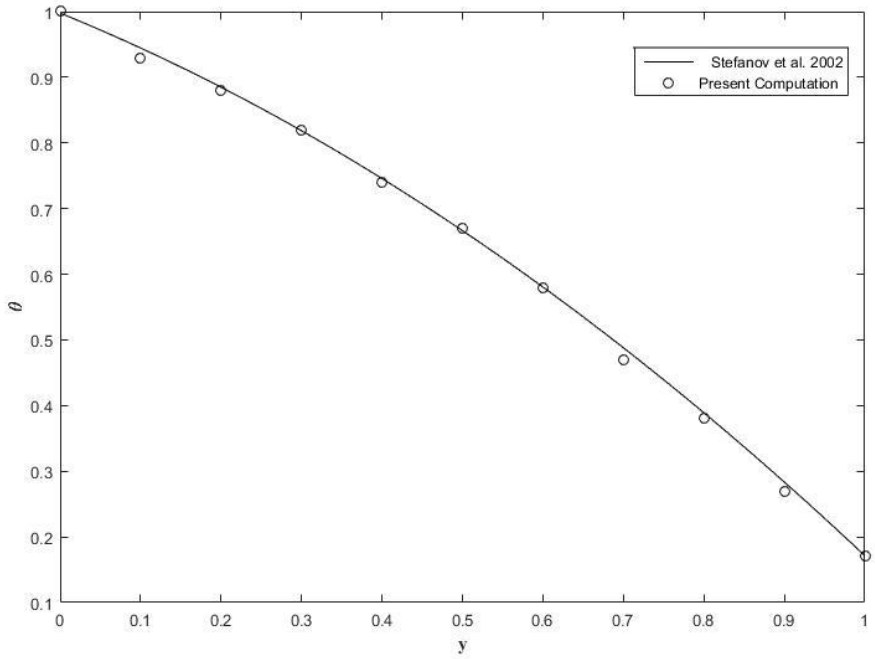

Figure 2.2: The temperature profiles for Kn = 0.005 & Fr=1

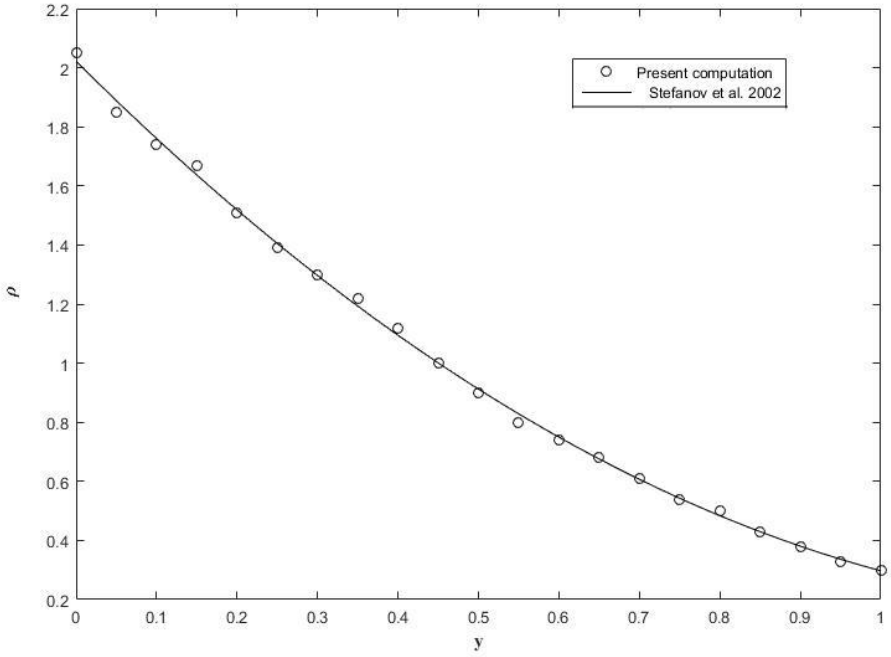

Figure 2.3: The density profiles for Kn = 0.005 & Fr=1

2.4 Discussion on Pure Conduction State

In this section, we shall analyze the effect of rarefaction (Kn), gravity as an external force (Fr), and accommodation coefficient (χ) on the pure conduction state. In the present analysis, we focused on large temperature difference between the plates and took $R_T = 0.1$.

2.4.1 Temperature Distribution

Figure 2.4 and 2.5 show the change in the temperature along the y-axis for different Kn at small and large values of Fr respectively. The verical arrows indicate the temperature-jump at specified values of Kn. Both figures suggest that the jump in the temperature increases as Kn becomes larger.

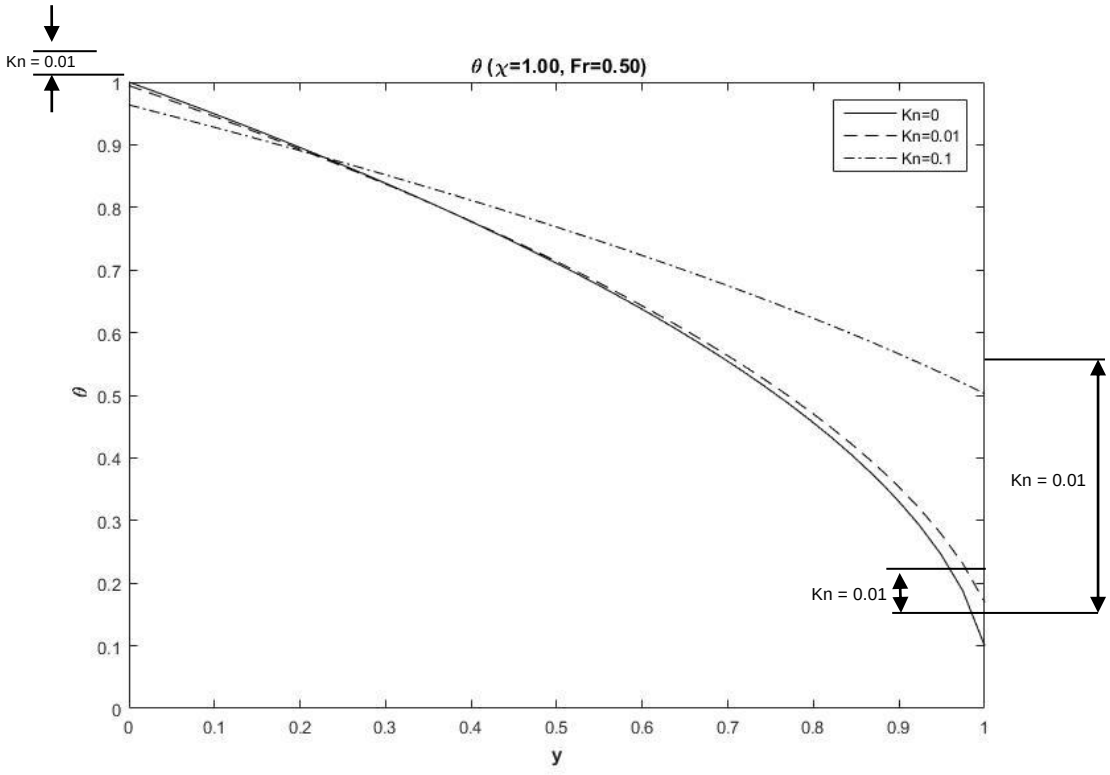

Figure 2.4: The temperature distribution for different Kn at Fr=0.5

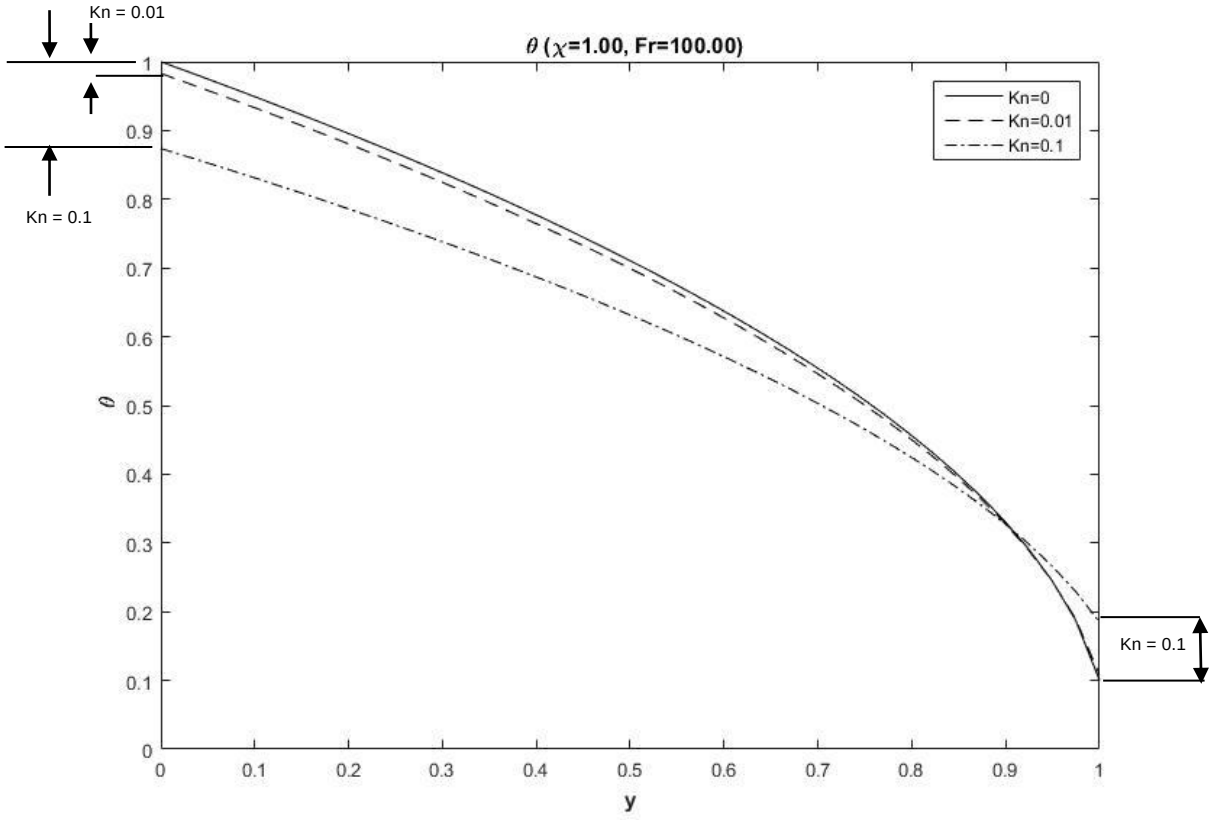

Figure 2.5: The temperature distribution for different Kn at Fr=100

At low level of rarefaction (very small Knudsen number, Kn→0), the temperature of the gas is exactly the same as that of the boundaries because of the absence of any temperature-jump. When the gas is moderately rarefied (i.e. Kn = 0.01), the effect of temperature jump is observed, and this jump increases with the increase in rarefaction (Kn). At high degree of rarefaction, (for large Kn, i.e. Kn = 0.1), the jump in the temperature becomes significantly high as shown in Figure 2.4 and 2.5. It is interesting to note that, the temperature-jump is noticably smaller at one boundary than the other. Under strong gravity, Fr = 0.5, the jump at the bottom plate (Figure 2.4) is less than the jump in the temperature under weak gravity, Fr = 100 (Fgure 2.5). When Fr is small, the gas particles are pulled downwards by storng gravity and tend to stagger near the bottom plate allowing more thermalization than at the upper plate.

Figure 2.6 & 2.7 show the effect of Fr on the temperature distribution at Kn = 0.01 and Kn = 0.1. When the gas is slightly rarefied, the effect of changing the thermal speed or gravity (Fr) on the temperature profiles is negligible (Figure 2.6). But, at higher degree of rarefaction (Kn = 0.1), the effect of Fr is significant on the temperature distribution of the gas (Figure 2.7). Considerable jump in the temperature is observed at both plates.

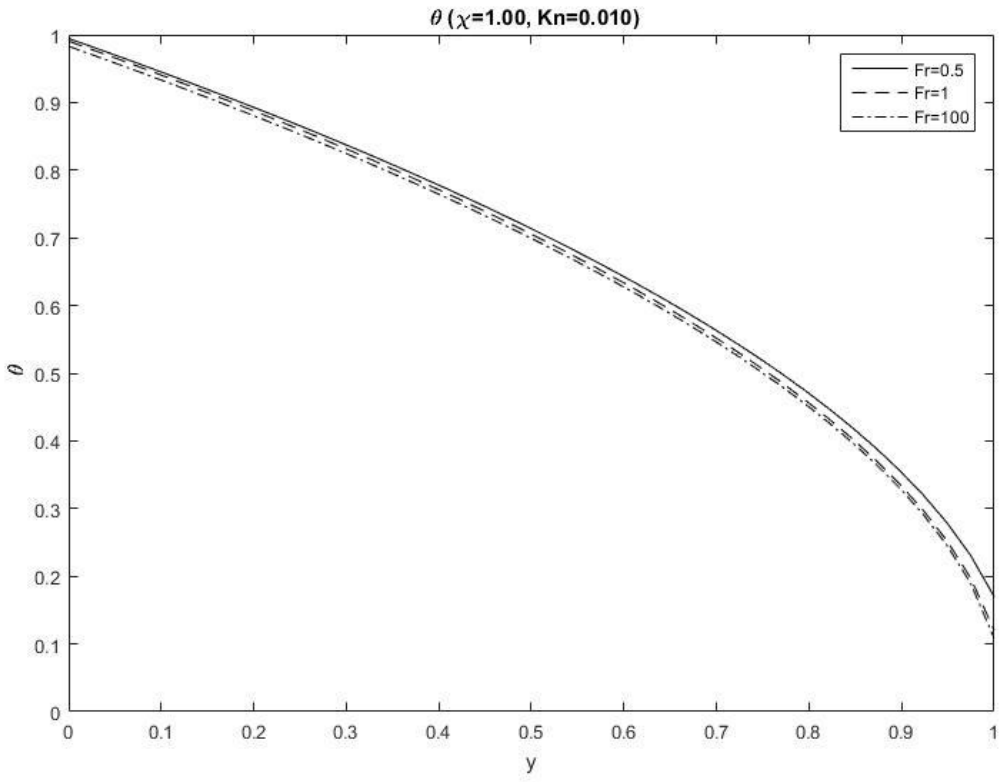

Figure 2.6: Effect of Fr on the temperature distribution at Kn = 0.01

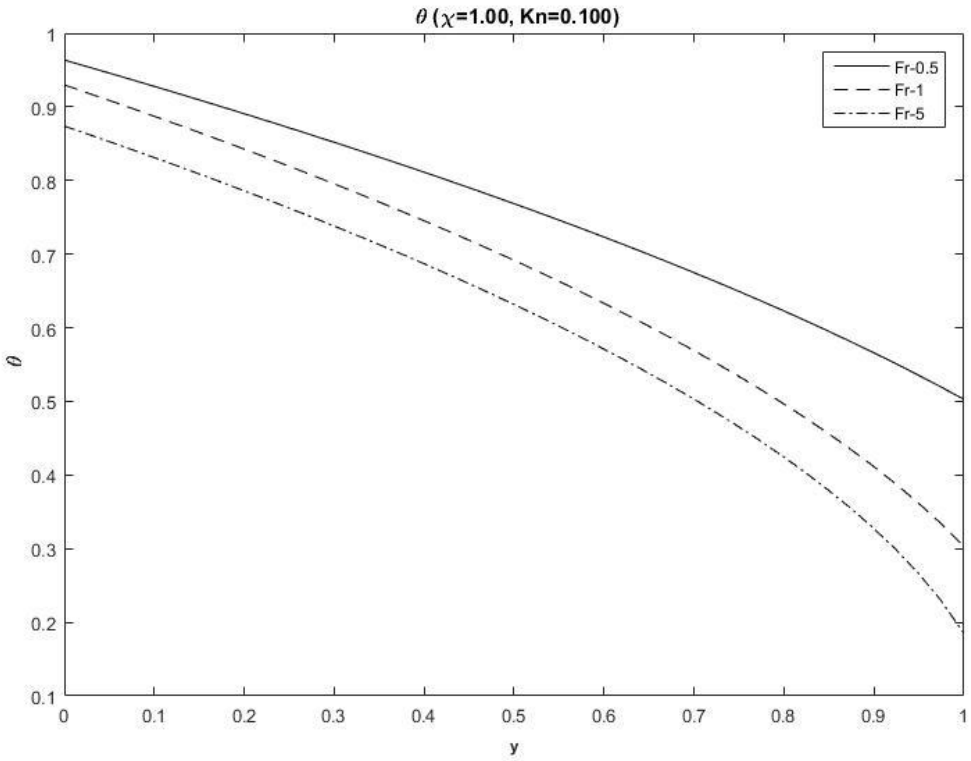

Figure 2.7: Effect of Fr on the temperature distribution at Kn = 0.1

Figure 2.8 & 2.9 show the effect of accommodation coefficient on the temperature jump for Kn = 0.01 under strong (i.e. Fr = 0.5) and weak gravity (i.e. Fr = 100), respectively. For full accommodation, $\chi = 1$, no jump in the temperature at the boundaries is observed. At partial accommodation, i.e. $\chi = 0.8$, temperature-jump is observed. As χ decreases, the temperature-jump increases significantly since a large fraction of gas molecules are specularly reflected allowing less gas particles to get thermalized with plates.

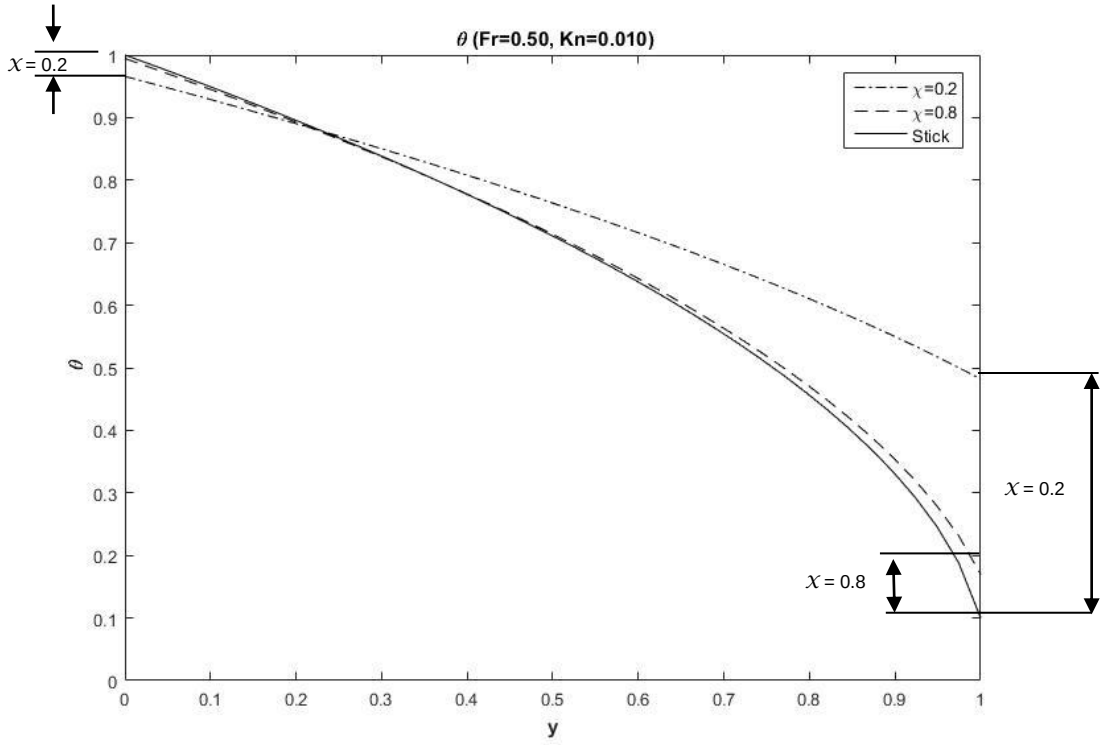

Figure 2.8: Effect of χ on the temperature jump at Kn = 0.01 & Fr = 0.5

At small Fr, due to strong gravitational effects, particles at the upper plate cannot thermalize with the plate and a higher temperature-jump is observed (Figure 2.8) than that in the case of a larger Fr (Figure 2.9).

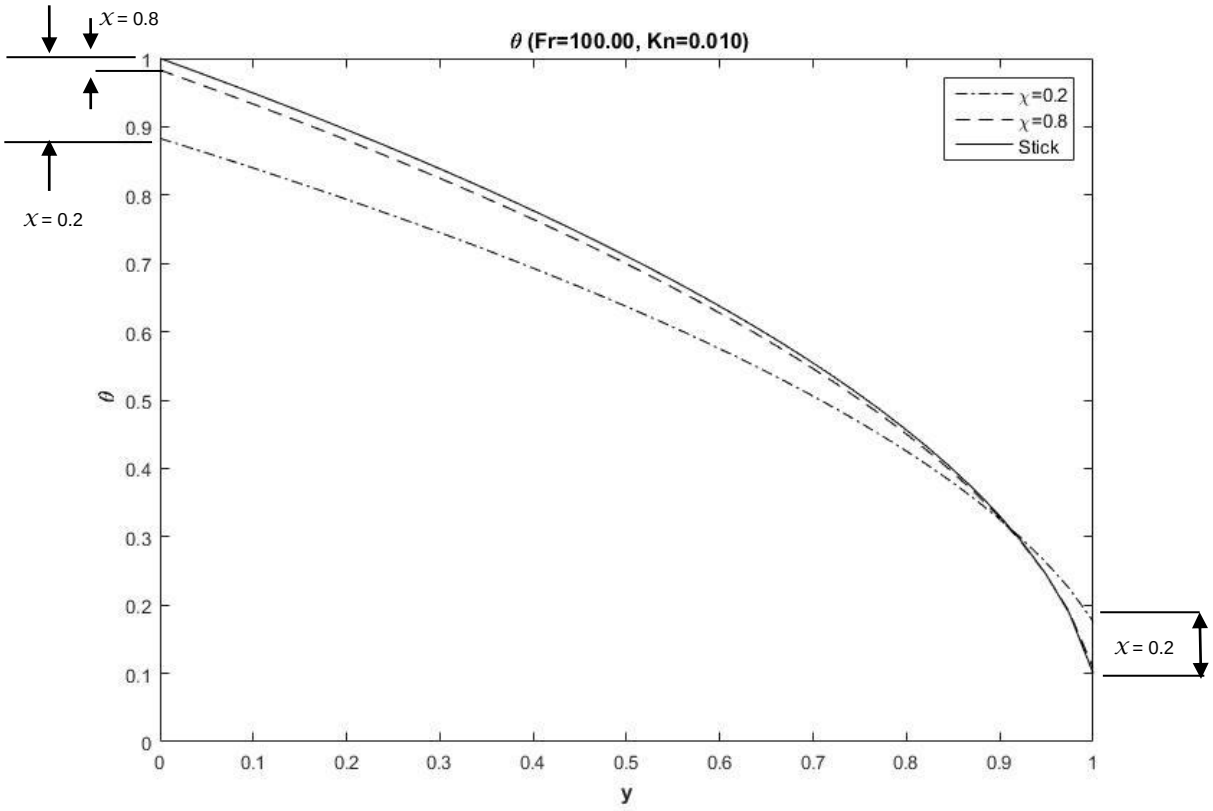

Figure 2.9: Effect of χ on the temperature jump at Kn = 0.01 & Fr=100

2.4.2 Heat Flux

Figure 2.10 & 2.11 present the heat flux across the gas domain at different degree of rarefaction for Fr = 0.5 and Fr = 100. A high value of heat flux is observe at the hot-bottom plate which continuosly decreases as we go towards the cold-top plate. The rate of heat transfer also decreases as the gas becomes more rarefied.

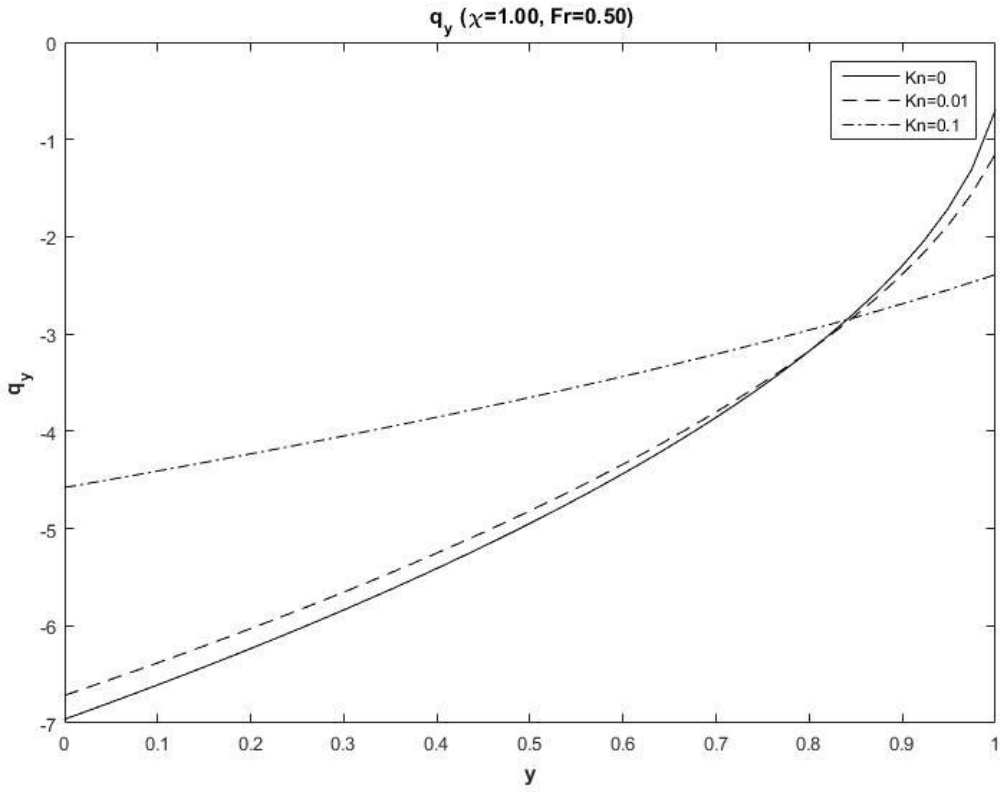

Figure 2.10: The variation of heat flux for different Kn at Fr =0.5

Since the heat flux depends on the temperature gradient and a large temperature-jump is observed near the top plate at higher degree of rarefaction (Figure 2.4), the heat transfer rate is higher for Kn = 0.1 (Figure 2.10). But, when the temperature-jump diminishes at large Fr (Figure 2.5), the heat flux becomes almost same for any degree of rarefaction in the gas at the top plate (Figure 2.11).

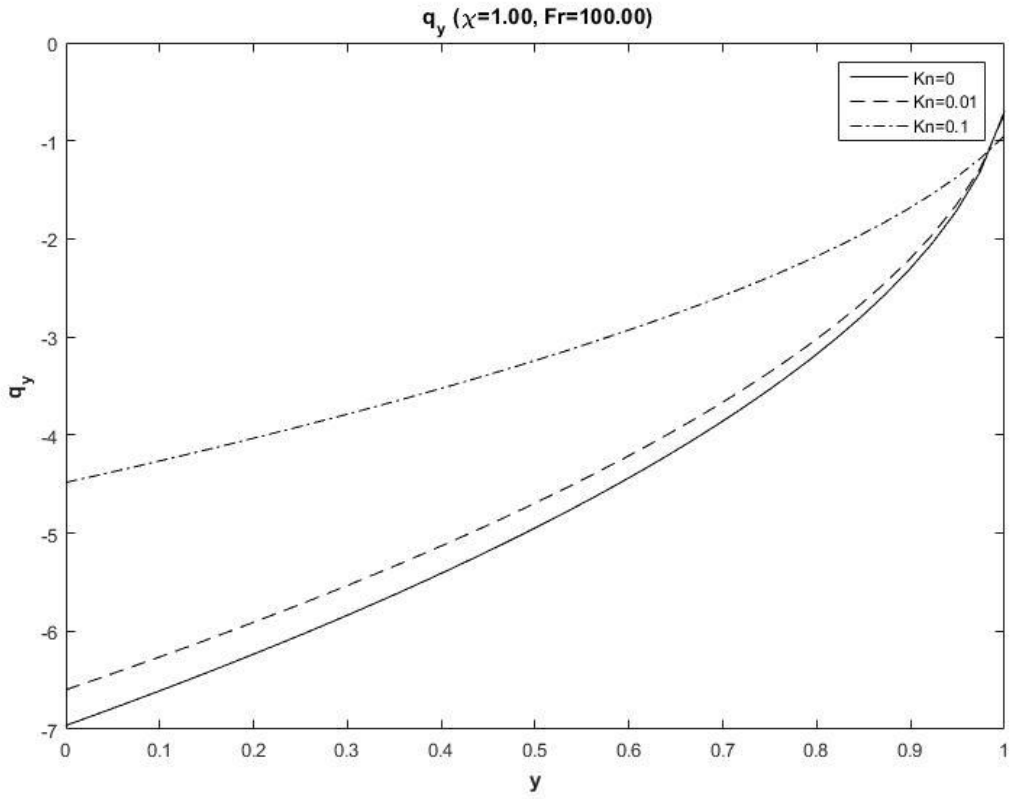

Figure 2.11: The variation of heat flux for different Kn at Fr=100

2.4.3 Density Distribution

Figure 2.12 & 2.13 show the density distribution for different degree of rarefaction at Fr = 0.5 and Fr = 100. Density distribution is not much affected by gas rarefaction except for the regions near the plates. In this region, variations in the density for different values of Kn are due to the fact that there exists a temperature-jump which depends on Kn. Since the jump in the temperature is higher for large Kn, the temperature of the gas near the hot-bottom plate is actually less than that of the plate. As a result, the density is slightly higher at large Kn near the bottom plate. Similarly, because of the existence of larger temperature-jump at large Kn, the temperature of the gas near the upper plate is higher than that of the plate which results in lower density of the gas.

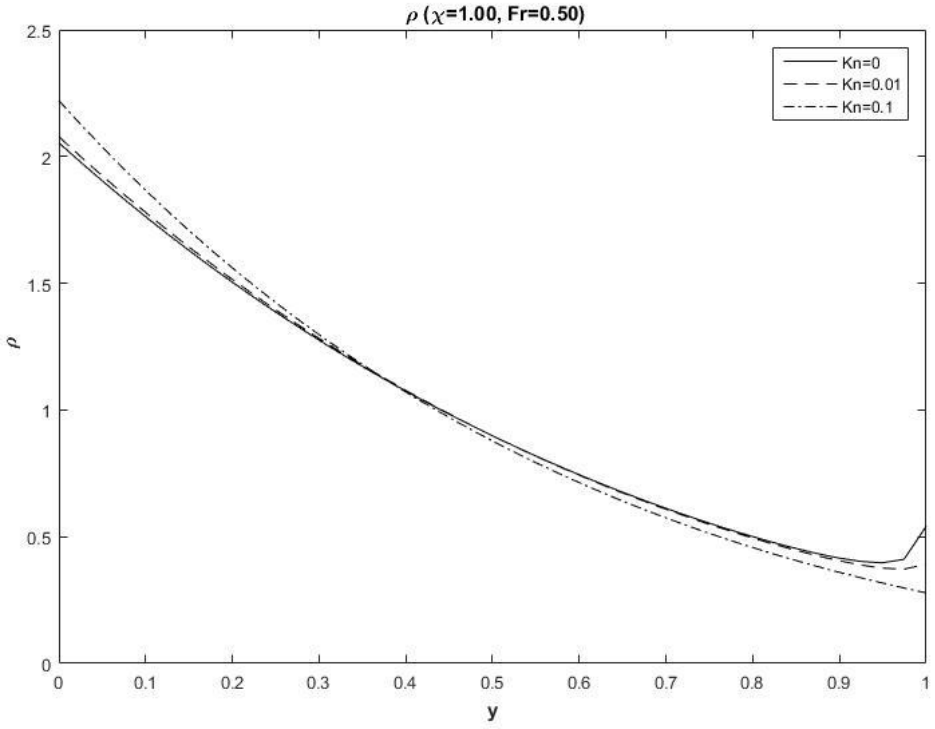

Figure 2.12: Density distribution for different Kn at Fr = 0.5

It is interesting to note that, even though the temperature of the gas near the bottom plate is higher than the gas near the top plate, the density can be higher near the bottom plate

for small values of Fr (Figure 2.12). This is due to the effects of compressibility-induced density variation.

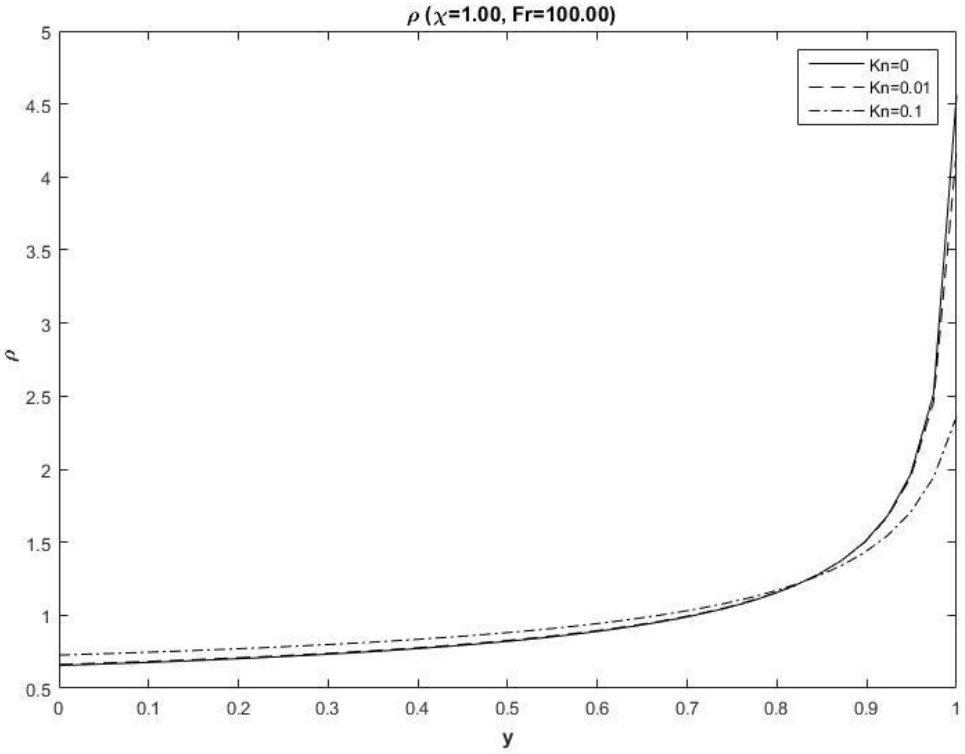

Figure 2.13: Density distribution for different Kn at Fr = 100

Figure 2.14 shows the effect of Fr on the density distribution for Kn = 0.01. At large Fr, the density follows a monotonically increasing trend with lighter fluid near the hot-bottom plate and denser fluid near the cold-top plate. Since the gravitational effect is small at large values of Fr, the pressure distribution becomes nearly uniform across the fluid layer (Figure 2.15) and compressibility effects become negligible. But, at small Fr, when the gravitational effect is much prominent, compressibility effects associated with the hydrostatic pressure distribution become important. As a result, higher density is observed near the hot-bottom plate and the density profile follows a monotonically decreasing trend as we go toward the top plate. At some intermediate value of the Froude number (Fr = 1), a nonmonotonical density distribution is obtained where the density decreases up to a finite distance from the bottom plate and then starts increasing towards the top plate.

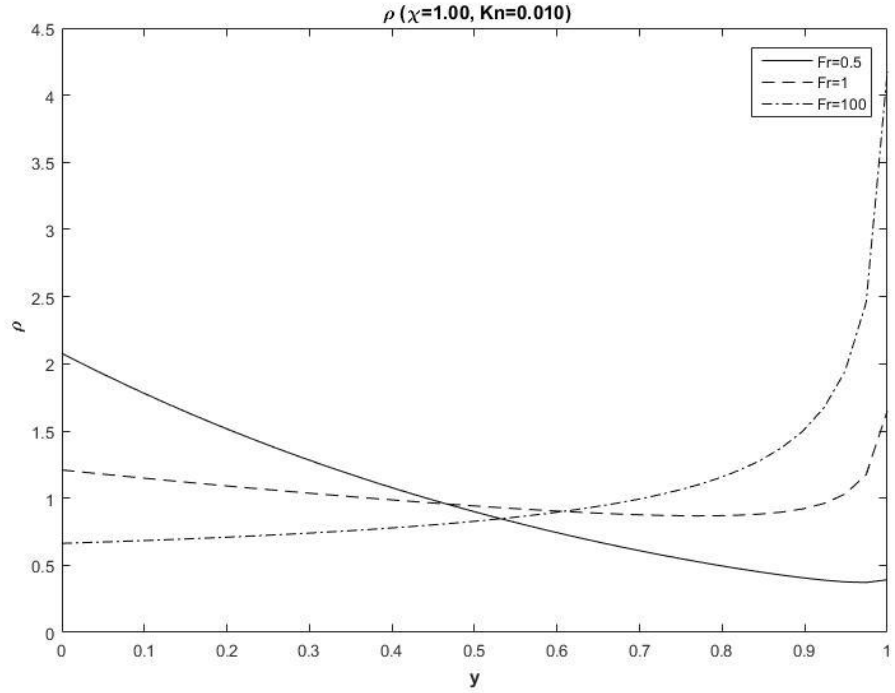

Figure 2.14: Effect of Fr on the density distribution at Kn=0.01

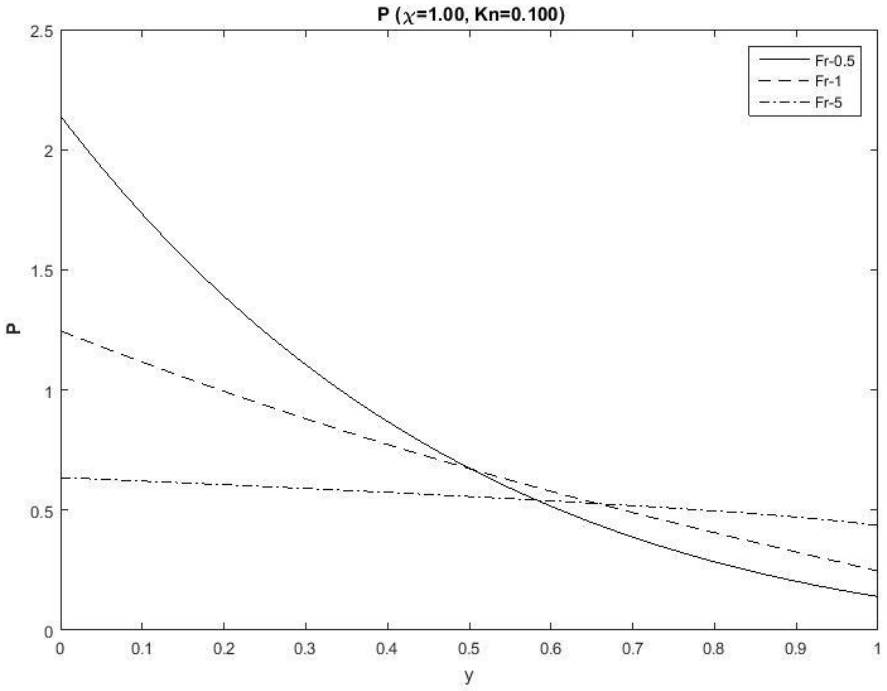

Figure 2.15: Effect of Fr on the pressure distribution at Kn=0.01

2.5 Comparison with Hard Sphere Model

The temperature of the steady pure conduction state as obtained by Stefanov et al. (2002) for hard sphere model does not depend on Fr, but from the present analysis using the Mawellian Molecules for predicting gas-solid interaction, it is evident that temperature distribution and temperature-jump at the both walls depend on Fr. At small Fr, when the thermal speed is less and the gravitational effect is stronger, the gas particles tend to stagger near the bottom plate and hence the temperature jump tends to be very small as compared that for a large Fr. On the other hand, the opposite phenomena are observed at the top plate.

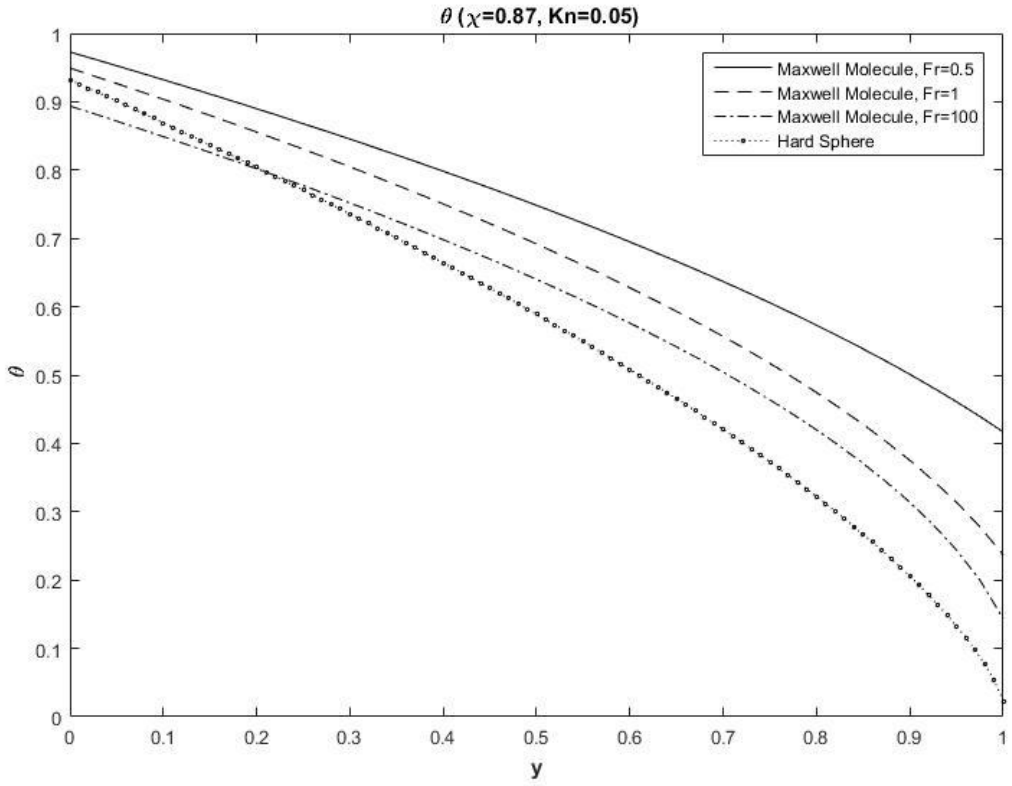

Figure 2.16: Temperature distribution for hard sphere and Maxwell models

2.6 Summary

The effect of rarefaction on the temperature-jump in a steady conduction state has been presented. With the increase in Kn, the temperature of the gas shows larger deviation from that of the plates. However, the jump in the temperature can be sigficanlty higher at the upper plate than the temperature-jump at the bottom plate at small Fr. Since the gas near the top weighs heavily down on the gas at the bottom under strong gravitational effect at small Fr, the gas is stratified in such a way that the density is higher near the bottom even with a higher temperature of the bottom plate. At large Fr, in the case of weak gravity, the density increases when moving towards the cold top plate while for some intermediate values of Fr, the density of the gas actually shows a nonmonotonic trend. At the end of the chapter, comparison between the hard-sphere and the Maxwell molecule has been presentd. While the present study based on the Maxwell molecules acknowledges the compressibility induced density variation and its effects on the temperature-jump, the results obtained by Stefanov et al. (2002) and Manela & Frankel (2005) using the hard-sphere model do not ackonwledge the Fr dependence of the temperature distribution.

Chapter 3

3 The Onset of Convection

The basic state considered in chapter 2 consists of a rarefied gas confined between two plates kept at different temperatures. Since the temperature of the bottom plate is higher than the upper plate, the lighter gas particles near the bottom plate tend to move up because of buoyancy. The upward movement of the gas is opposed by the viscous dissipation, thermal diffusion by conduction, and the compressibility of the gas. The governing equations are given in (2.1) to (2.3) along with the boundary conditions (2.11) and (2.12). In the absence of convection, the gas is at rest and heat transfer takes place by pure conduction. The base state, the pure conduction in the present case, is governed by the linear momentum equation and energy equation in the vertical direction (2.21) and (2.22), and the boundary conditions are given by the temperature-jump condition at both plates (2.25) and (2.26).

3.1 Problem Formulation

Conditions leading to the onset of convection is determined by using linear stability analysis where small perturbations in the velocity, temperature, pressure, or density are added to the base state. If the perturbation grows in time, the system is said to be unstable and convection sets in. On the other hand, if the perturbation decays in time, pure conduction state prevails. To mathematically analyze the stability of the system, the perturbation is represented in terms of a Fourier series expansion as the perturbation is a superposition of normal modes. Rather than studying a perturbation of arbitrary form, all possible normal modes are checked to determine if the system is stable. If any mode is found to grow in time, the system is called unstable since in a perturbation of infinitesimal amplitude, every possible mode will always be present.

To analyze the linear temporal stability of the pure-conduction state for our problem, the base state is perturbed by small spatially harmonic perturbations which are represented by

$$\left.\begin{aligned} u(t,x,y) &= u_b(y) + u(y)e^{st+ikx}, \\ v(t,x,y) &= v_b(y) + v(y)e^{st+ikx}, \\ \rho(t,x,y) &= \rho_b(y) + \rho(y)e^{st+ikx}, \\ \text{and, } \theta(t,x,y) &= \theta_b(y) + \theta(y)e^{st+ikx}, \end{aligned}\right\} \tag{3.1}$$

where superscript b denotes the base state and since there is no flow at the base state, $u_b(y) = v_b(y) = 0$. Here k is the wave number in the direction of x and s is the frequency of the perturbation. In a temporal stability analysis problem, the spatial structure of the wavelike perturbation is unchanged and the amplitude of the wave grows or decays as time progresses. The wave number k is taken to be real whereas the frequency $s = \sigma + i\omega$ is chosen as complex. The system remains stable if $\sigma < 0$ and loses its stability if $\sigma > 0$. It is said to be neutrally stable if $\sigma = 0$. If $\omega = 0$, the transition to instability takes place via 'exchange of stabilities' and exhibits stationary patterns of motion. But when $\omega \neq 0$, the instability sets in exhibiting oscillatory motions with a definite characteristic frequency.

To develop the governing equations in the perturbation problem, expressions in (3.1) were substituted in the nondimensional governing equations (2.10) – (2.12) and making use of the equation of state (2.13), pressure p was eliminated. After neglecting all the nonlinear terms, the perturbation problem consists of the following set of equations

$$s\rho + ik\rho_b u + \rho_b \frac{\partial v}{\partial y} + \frac{d\rho_b}{dy} v = 0, \tag{3.2}$$

$$\begin{aligned} \rho_b s u = &-ik\rho_b\theta - ik\theta_b\rho - Kn\left[-\frac{4}{3}k^2\theta_b u + \frac{2}{3}ik\theta_b\frac{\partial v}{\partial y}\right] \\ &-Kn\left[-\theta_b\frac{\partial^2 u}{\partial y^2} - \frac{d\theta_b}{dy}\frac{\partial u}{\partial y} - ik\theta_b\frac{\partial v}{\partial y} - ik\frac{d\theta_b}{dy}v\right], \end{aligned} \tag{3.3}$$

$$\rho_b s v = -\left(\rho_b \frac{\partial \theta}{\partial y} + \rho \frac{d\theta_b}{dy}\right) - \left(\theta_b \frac{\partial \rho}{\partial y} + \theta \frac{d\rho_b}{dy}\right) - Kn\left[k^2 \theta_b v - ik\theta_b \frac{\partial u}{\partial y}\right]$$
$$-Kn\left[-\frac{4}{3}\theta_b \frac{\partial^2 v}{\partial y^2} - \frac{4}{3}\frac{d\theta_b}{dy}\frac{\partial v}{\partial y} + \frac{2}{3}ik\theta_b \frac{\partial u}{\partial y} + \frac{2}{3}ik\frac{d\theta_b}{dy}u\right] - \frac{1}{Fr}\rho, \tag{3.4}$$

$$\frac{3}{2}\rho_b s\theta + \frac{3}{2}\rho_b \frac{d\theta_b}{dy} v = \frac{15}{4} Kn\left[-k^2\theta_b\theta + \theta_b \frac{\partial^2 \theta}{\partial y^2} + \theta \frac{d^2\theta_b}{dy^2} + 2\frac{d\theta_b}{dy}\frac{\partial \theta}{\partial y}\right]$$
$$-ik\rho_b\theta_b u - \rho_b\theta_b \frac{\partial v}{\partial y} \tag{3.5}$$

along with the boundary conditions for the perturbation equations developed from (2.15) and (2.16)

$$\left.\begin{aligned} &Kn\left(\theta_b\right)^{\frac{1}{2}} \frac{\partial u}{\partial y} = \frac{\chi}{2-\chi}\sqrt{\frac{2}{\pi}}\rho_b u, \\ &v = 0, \text{ and}, \\ &\frac{15}{4}Kn\left(\theta_b \frac{\partial \theta}{\partial y} + \theta \frac{d\theta_b}{dy}\right) = \frac{2\chi}{2-\chi}\sqrt{\frac{2}{\pi\theta_b}}\left(\rho\theta_b\theta_b - \rho\theta_b\theta_W + \frac{3}{2}\theta\rho_b\theta_b - \frac{1}{2}\theta\rho_b\theta_W\right) \end{aligned}\right\} \tag{3.6}$$

at the bottom hot plate, and

$$\left.\begin{aligned} &Kn\left(\theta_b\right)^{\frac{1}{2}} \frac{\partial u}{\partial y} = -\frac{\chi}{2-\chi}\sqrt{\frac{2}{\pi}}\rho_b u, \\ &v = 0, \text{ and}, \\ &\frac{15}{4}Kn\left(\theta_b \frac{\partial \theta}{\partial y} + \theta \frac{d\theta_b}{dy}\right) = -\frac{2\chi}{2-\chi}\sqrt{\frac{2}{\pi\theta_b}}\left(\rho\theta_b\theta_b - \rho\theta_b\theta_W + \frac{3}{2}\theta\rho_b\theta_b - \frac{1}{2}\theta\rho_b\theta_W\right) \end{aligned}\right\} \tag{3.7}$$

at the upper cold plate.

Together with the boundary conditions (3.6) and (3.7), the set of perturbation equations (3.2) – (3.5) forms an eigenvalue problem where only specific combinations of s, k, Kn,

Fr, and R_T give non-trivial solutions to the problem. To calculate the dispersion relation $s = s(k; Kn, Fr, R_T)$, the set of differential equations (3.2) – (3.5) were transformed into an algebraic eigenvalue problem using Chebyshev collocation method.

The solution of (3.2) – (3.7) involves approximating each of the variables u, v, ρ, and θ in terms of Chebyshev polynomials which can be written in the form

$$u_N(x) = \sum_{k=0}^{N} \hat{u}_k T_k(x) \tag{3.8}$$

where $\hat{u}_k$ is the coefficient associated with the expansion, and $T_k(x)$ are the Chebyshev polynomial of degree k defined by

$$T_k(x) = \cos\left(k \cos^{-1} x\right), \qquad k = 0,1,2,... \tag{3.9}$$

in the interval $x \in [-1,1]$. According to the collocation method, solution of the differential equations is exactly satisfied by the approximating polynomial $u_N(x)$ at the collocation points

$$x_i = \cos\frac{\pi i}{k}, \quad i = 0,...,k. \tag{3.10}$$

In the set of equations and the boundary conditions (3.2) – (3.7), the field variables and their derivatives are then expressed in terms of $u_N(x_i)$. The p^{th} derivative is calculated by

$$u_N^{(p)}(x_i) = \sum_{j=0}^{N} d_{i,j}^{(p)} u_N(x_j), \qquad i = 0,...., N \tag{3.11}$$

where the coefficients $d_{i,j}^{(p)}$ can be easily calculated making use of the fact that the Chebyshev polynomial defined above is basically a trigonometric function (Peyret 2002).

Before writing the governing equations of the perturbations in terms of the approximating polynomials and their derivatives using the (3.9) and (3.11), the domain in the y direction was transformed from [0, 1] to [-1, 1]. Also, to avoid handling the complex number i in the governing equations, we chose $f = iku$. The transformed equations read as follow:

$$(s)\rho_N + (\rho_b) f_N + \left(2\rho_b \sum_{j=0}^{N} d'_{i,j}\right) v_N + (\rho_b') v_N = 0$$

$$(-s\rho_b) f_N + \left(\frac{4}{3}k^2 Kn\theta_b\right) f_N + \left(2Kn\theta_b' \sum_{j=0}^{N} d'_{i,j}\right) f_N + \left(4Kn\theta_b \sum_{j=0}^{N} d''_{i,j}\right) f_N$$
$$+ \left(-k^2 Kn\theta_b'\right) v_N + \left(-\frac{2}{3}k^2 Kn\theta_b \sum_{j=0}^{N} d'_{i,j}\right) v_N + \left(k^2\theta_b\right) r_N + \left(k^2\rho_b\right)\theta_N = 0$$

$$\left(-\frac{2}{3}Kn\theta_b'\right) f_N + \left(\frac{2}{3}Kn\theta_b \sum_{j=0}^{N} d'_{i,j}\right) f_N$$
$$+ (-s\rho_b) v_N + \left(-k^2 Kn\theta_b\right) v_N + \left(\frac{8}{3}Kn\theta_b' \sum_{j=0}^{N} d'_{i,j}\right) v_N + \left(\frac{16}{3}Kn\theta_b \sum_{j=0}^{N} d''_{i,j}\right) v_N$$
$$+ (-F)\rho_N + (-\theta_b')\rho_N + \left(-2\theta_b \sum_{j=0}^{N} d'_{i,j}\right)\rho_N + (-\rho_b')\theta_N + \left(-2\rho_b \sum_{j=0}^{N} d'_{i,j}\right)\theta_N = 0$$

$$(-\rho_b\theta_b) f_N + \left(-\frac{3}{2}\rho_b\theta_b'\right) v_N + \left(-2\rho_b\theta_b \sum_{j=0}^{N} d'_{i,j}\right) v_N$$
$$+ \left(-\frac{3}{2}s\rho_b\right)\theta_N + \left(-\frac{15}{4}k^2 Kn\theta_b\right)\theta_N + \left(\frac{15}{4}Kn\theta_b''\right)\theta_N$$
$$+ \left(15Kn\theta_b' \sum_{j=0}^{N} d'_{i,j}\right)\theta_N + \left(15Kn\theta_b \sum_{j=0}^{N} d''_{i,j}\right)\theta_N = 0$$

along with the boundary conditions

$$\left.\begin{aligned}
&\left(2\mathrm{Kn}\theta_b^{\frac{1}{2}}\sum_{j=0}^{N} d'_{1,j}\right) f_N = \left(\frac{\chi}{2-\chi}\sqrt{\frac{2}{\pi}}\rho_b\right) f_N, \\
&v_N = 0, \text{ and}, \\
&\left(\frac{15}{2}\mathrm{Kn}\theta_b\sum_{j=0}^{N} d'_{i,j}\right)\theta_N + \left(\frac{15}{4}\mathrm{Kn}\theta_b{}'\right)\theta_N \\
&\qquad = \left(\frac{2\chi}{2-\chi}\sqrt{\frac{2}{\pi}}\right)\theta_b{}^{-\frac{1}{2}}\left[\left(\theta_b{}^2\right)\rho_N - \left(\theta_b\theta_W\right)\rho_N + \frac{3}{2}\left(\rho_b\theta_b\right)\theta_N - \frac{1}{2}\left(\rho_b\theta_W\right)\theta_N\right]
\end{aligned}\right\}$$

at the bottom hot plate and

$$\left.\begin{aligned}
&\left(2\mathrm{Kn}\theta_b^{\frac{1}{2}}\sum_{j=0}^{N} d'_{1,j}\right) f_N = -\left(\frac{\chi}{2-\chi}\sqrt{\frac{2}{\pi}}\rho_b\right) f_N, \\
&v_N = 0, \text{ and}, \\
&\left(\frac{15}{2}\mathrm{Kn}\theta_b\sum_{j=0}^{N} d'_{i,j}\right)\theta_N + \left(\frac{15}{4}\mathrm{Kn}\theta_b{}'\right)\theta_N \\
&\qquad = -\left(\frac{2\chi}{2-\chi}\sqrt{\frac{2}{\pi}}\right)\theta_b{}^{-\frac{1}{2}}\left[\left(\theta_b{}^2\right)\rho_N - \left(\theta_b\theta_W\right)\rho_N + \frac{3}{2}\left(\rho_b\theta_b\right)\theta_N - \frac{1}{2}\left(\rho_b\theta_W\right)\theta_N\right]
\end{aligned}\right\}$$

at the upper cold plate.

The transformed problem then consists of a system of 4N linear equations satisfied by the perturbations at N discrete points across the gas domain. Since, we are interested to obtain the marginal stability curve, s was taken to be zero. For a particular wave number, k, to find the eigenvalues, a specific value of Kn was chosen and the determinant was calculated each time for different Fr until the determinant became zero. The combination of Kn and Fr which made the determinant zero was recorded. The calculations were repeated for different values of Kn to find the corresponding Fr to construct the marginal

stability curve. Similar to the study by Manela & Frankel (2005), the convergence of the calculation has been established for N = 70 (Figure 3.1).

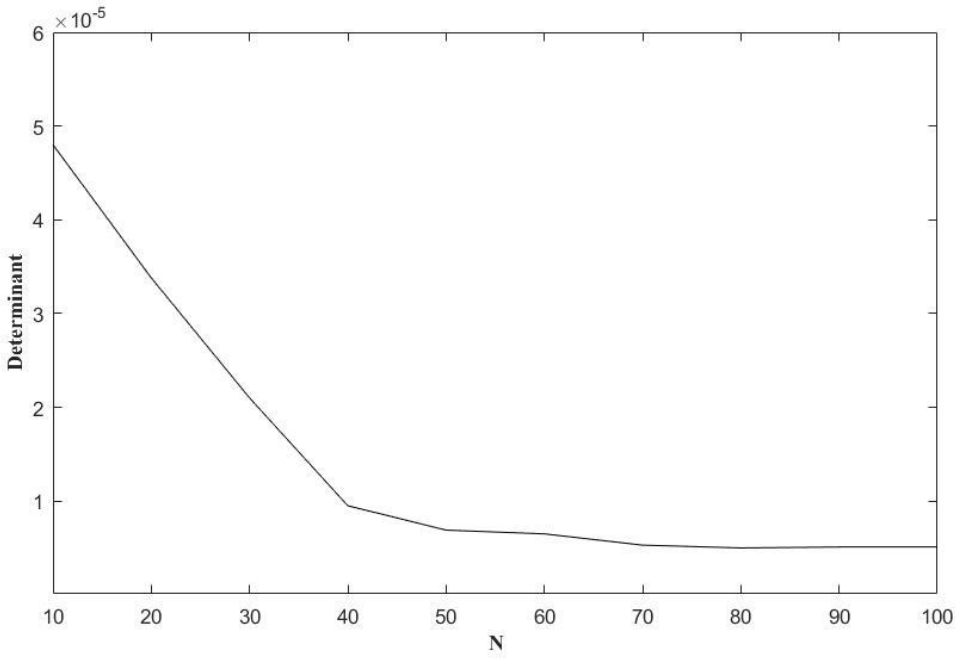

Figure 3.1: Convergence test

The accuracy of the numerical technique employed for the solution of the eigenvalue problem was checked by solving the problem formulated by Manela and Frankel (2005). A marginal stability curve obtained using the method described above along with that obtained by Manela and Frankel (2005) are shown in Figure 3.2. Both results are in excellent agreement which confirms the accuracy of the present work.

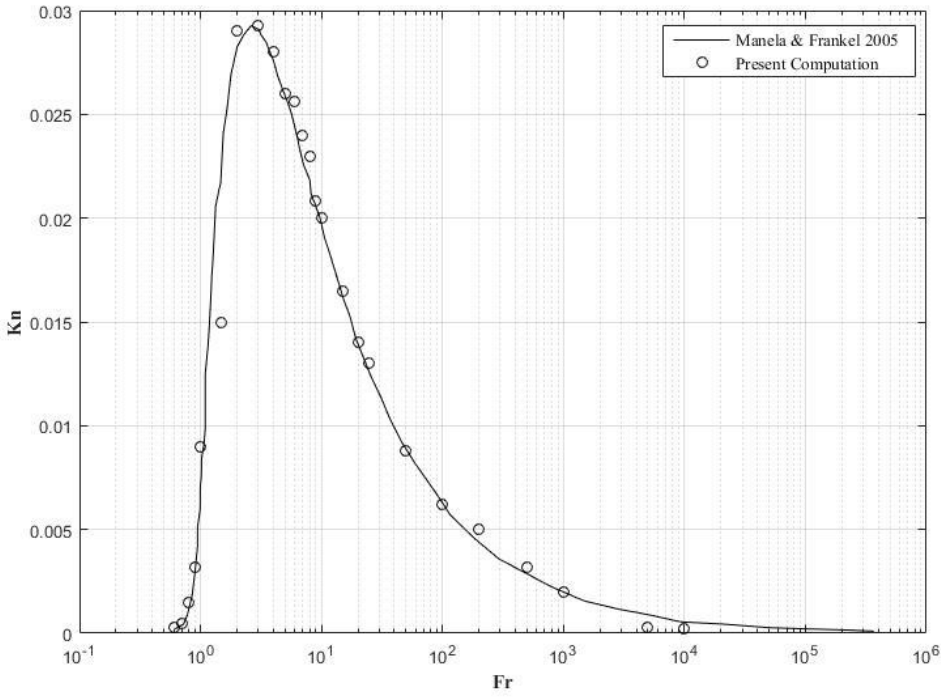

Figure 3.2: The marginal stability curve for a hard-sphere model

3.2 Results

Throughout the entire domain of parameters, the present computation invariably yield real-valued s, its positive value indicates convection sets in and a negative value indicates pure conduction state prevails. The following results have been presented for a temperature ratio, $R_T = 0.1$ and $k = 3.12 \approx \pi$ to facilitate comparison with the results of Manela & Frankel (2005). The choice of k = 3.12 is inspired by the critical wave number found by Chandrasekhar (1961) for an incompressible fluid with Boussinesq approximation. Later, Jeng & Hassard (1999) showed that the critical wave number for similar problem is unique. Recently, Barbera (2003) also found that the critical wave number for Rayleigh Bénard system with gases is also 3.12.

Figure. 3.3 shows the neutral curve in the (Fr, Kn) plane for $k = \pi$ and $R_T = 0.1$. The solid line in Figure 3.3 shows the separation of the (Fr, Kn) plane into the domains of unstable response, growth rate, s > 0, and stable response, s < 0.

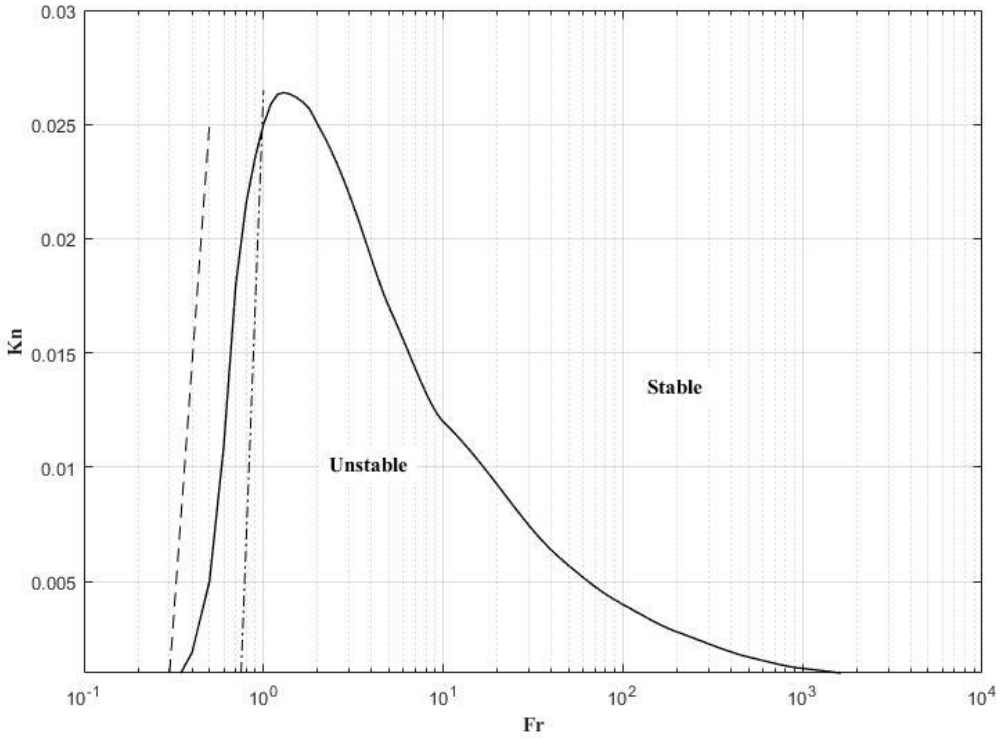

Figure 3.3: The marginal stability curve (solid line) marked with stable and unstable zone, the necessary condition for the onset of convection (dashed line), and the initial appearance of nonmonotonic density distribution (dash-dotted line)

The dash-dotted line marks the initial appearances of nonmonotonic density distribution in the pure conduction state (Figure 3.3). To the right of this line, the density of the gas increases monotonically which gives an unstable configuration where the heavier fluid rests on top of the lighter fluid. In such arrangements, convection may set in easily as the heavier fluid falls back allowing the lighter fluid to rise under a temperature gradient large enough to overcome the viscous effects. On the left side of the dash-dotted line (Figure 3.3), the density is stratified in such a way that the lighter fluid rests on top of heavier fluid because of the compressibility effect even though the temperature at the bottom plate is higher. Although it seems to be a stable configuration, convection still can set in provided that adiabatic expansion of a fluid element reduces its density below the ambient reference density as the fluid element rises through the hydrostatic pressure field.

So for convection to take place, the vertical temperature gradient is required to satisfy the condition

$$\frac{dT}{dy} < -\frac{\alpha T g}{c_P} \tag{3.8}$$

where α is the thermal expansion coefficient and c_P is the specific heat at constant pressure. Condition (3.8) basically states that the vertical temperature gradient must be smaller than the adiabatic gradient corresponding to the ambient hydrostatic pressure (Landau & Lifshitz, 1959). In the present dimensionless notation, the condition reads

$$\Delta(y) = \frac{dT_b}{dy} + \frac{4}{5Fr} < 0 . \tag{3.9}$$

The condition (3.9) is satisfied on the right of the dash-dotted line where the density stratification is such that heavy fluid rests on top of light fluid giving rise to an unstable configuration, it is, however, interesting to note that the condition is also satisfied on the other side, between the neutral curve and the left of the dash-dotted line. For instance, for Kn = 0.01, the density changes its trend at Fr = 0.9. If we plot the condition (3.9) at two points just to the left and right of the dash-dotted line (Fr = 0.8 and Fr = 1) for Kn = 0.01, it is observed that (3.9) is satisfied near the upper cold plate in both cases (Figure 3.4). The hatched areas represent the region where convection sets in.

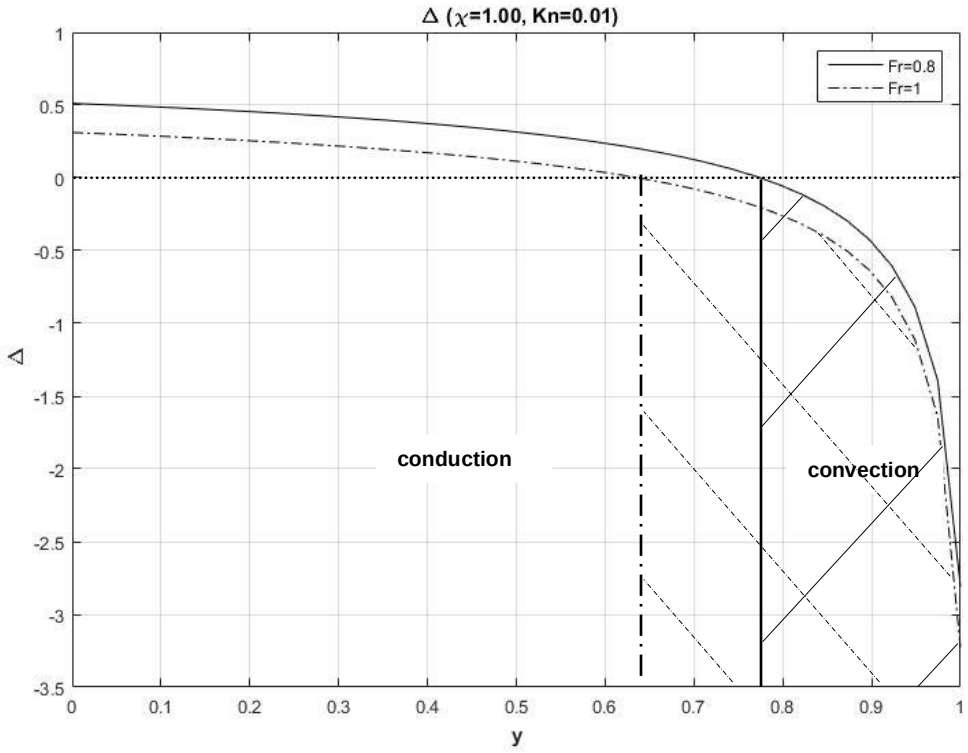

Figure 3.4: Onset of convection at small Fr

In Figure 3.3, the dashed line represents the locus of conditions where (3.9) is initially satisfied. However, (3.9) does not consider the retarding effects of viscosity and heat conductivity which is why it is, in fact, a necessary condition for the onset of convection, not the sufficient condition. As such, it is not surprising that the corresponding line appears to the left of actual boundary delineated by the neutral curve. According to condition (3.9), for Kn = 0.01 critical Fr for the onset of convection appears to be 0.4. But from the neutral curve obtained in the present linear stability analysis, it is seen that convection sets in for a value of Fr larger than 0.6 at Kn = 0.01. The condition is only satisfied at the upper cold plate for Fr = 0.4 (Figure 3.3). If we move to Fr = 0.6, the condition is satisfied throughout a finite distance from the upper cold plate and convection is sustained. As we move to higher Fr, convection extends over a wider area owing to viscous momentum diffusion to lower fluid layers. At Fr = 5, convection occupies the entire gas domain between the walls.

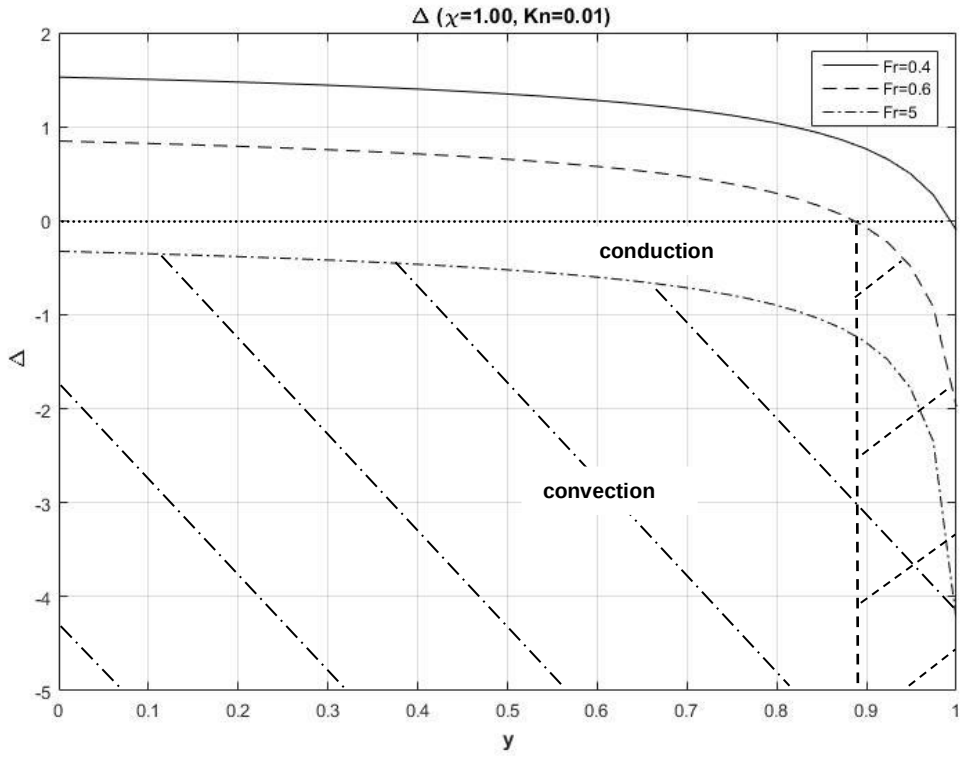

Figure 3.5: Necessary condition for the onset of convection

The finite distance from the upper cold plate, through which (3.9) must be satisfied for convection to set in, varies for different Knudsen number as can be seen from Figure 3.6. As we move along the left boundary of the neutral curve to larger Fr and Kn, the interval adjacent to the upper cold plate where the necessary condition (3.9) is satisfied widens. At Fr = 0.5 and Kn = 0.005, the distance from the upper plate where convection sets in is less than one-tenth of the total domain height whereas, at Fr = 0.8 and Kn = 0.02, this distance extends up to twice as much as the former one. These results are in qualitatively agreement with the flow structure shown in Stefanov et al. (2002). Their observation shows that the convection vortices form throughout the whole gas domain for all Kn on the right boundary. But, on the right boundary, due to strong gas stratification near the bottom plate, convection rolls tend to shift upwards from the hot bottom plate. For the lowest Kn = 0.001 and Fr =0.8 that they were able to study using the DSMC and finite difference method, the rolls only occupied one-third of the gas domain starting from the cold upper plate.

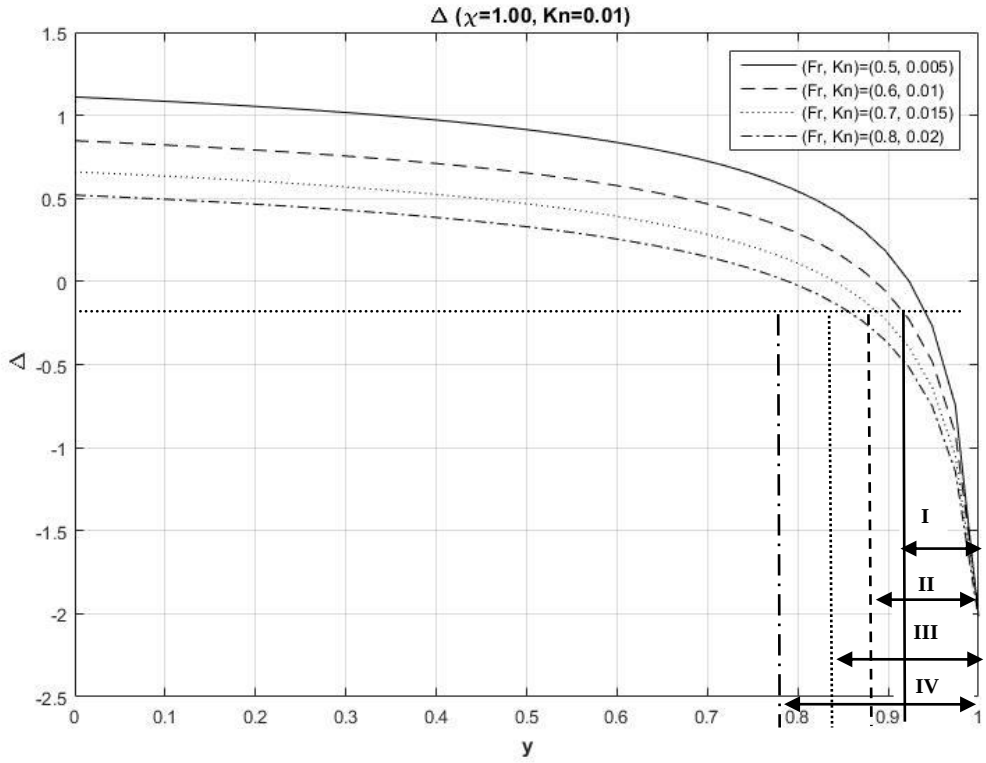

Figure 3.6: Span of convection zone at different points along the neutral curve

I. (Fr, Kn) = (0.5, 0.005), II. (Fr, Kn) = (0.6, 0.01), III. (Fr, Kn) = (0.7, 0.015), IV. (Fr, Kn) = (0.8, 0.02)

The neutral curve shown in Figure 3.3 indicates the stability of the Rayleigh-Bénard system for rarefied gases for $k = \pi$. The governing parameter in the case of an incompressible fluid is the Rayleigh number which is expressed as

$$\mathrm{Ra} = \frac{\rho_h \alpha_h T_h g (1 - R_T) D^3}{\kappa_h \mu_h} \quad . \tag{3.10}$$

Using the expressions for transport coefficients for a Maxwellian gas, the expression for the Rayleigh number can be written in terms of R_T, Fr and Kn as

$$\mathrm{Ra} = \frac{3}{2} \frac{1 - R_T}{\mathrm{Fr Kn}^2} . \tag{3.11}$$

The critical Ra number is not constant for rarefied gas unlike in the case of an incompressible fluid or even compressible ones within the framework of the Boussinesq approximation. Rather, there exist an upper and lower bound of Ra for which convection sets in.

The stability of a system can only be confirmed if it is stable under perturbations with all possible wave numbers. Even if the system is unstable for a single value of the wave number of the perturbation while being stable for all other wave numbers, the system cannot be called a stable system. Therefore, to determine the neutral stability of the Rayleigh-Bénard configuration in the present study, multiple neutral curves in (Fr, Kn) plane for different values of k have been obtained. Figure 3.7 shows the neutral curves for different values of wave number starting from $k = 0.5\pi$ to $k = 3\pi$. The lowest neutral curve corresponding to $k = 3\pi$ denoted by the dashed line. This indicates that for any combination of Fr and Kn inside the curve, a disturbance with a wave number of $k = 3\pi$ can make the conduction state unstable and convection can set in. For any points outside the neutral curve, such a disturbance cannot destabilize the conduction state. However, disturbances with a different wave number i. e. $k = 0.5\pi$, $k = \pi$ or $k = 2\pi$ may cause instability as shown in Figure 3.7. The neutral curve for $k = \pi$ encompasses all the other curves which means that if the conduction state is stable for a disturbance of wave number $k = \pi$, then the state is also stable for any other disturbances with different wave numbers. Therefore, $k = \pi$ is indeed the critical wave number for the onset of convection in a rarefied gas.

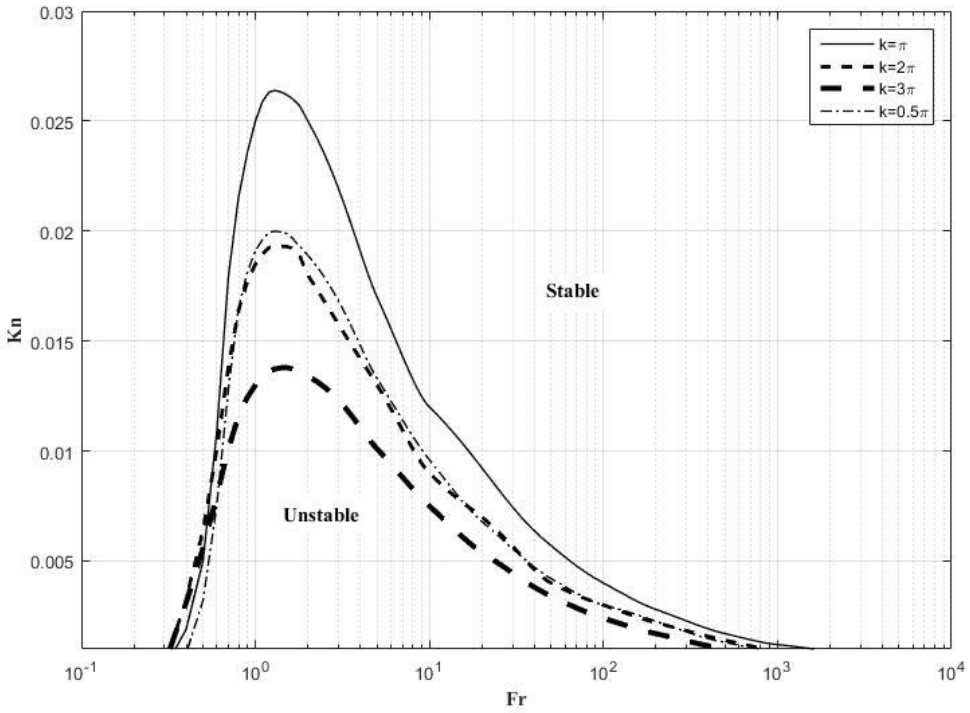

Figure 3.7: The neutral curves for different wave number

The minimum Rayleigh numbers which are responsible for the onset of convection for different wave numbers are plotted in Figure 3.8. It is observed that there is a minimum point in the curve plotted in Figure 3.6 which actually confirms that $k = \pi$ is indeed the critical wave number for the compressible Rayleigh-Bénard problem and the lowest value of Ra (which is 860) that could induce convection corresponds to this value of k.

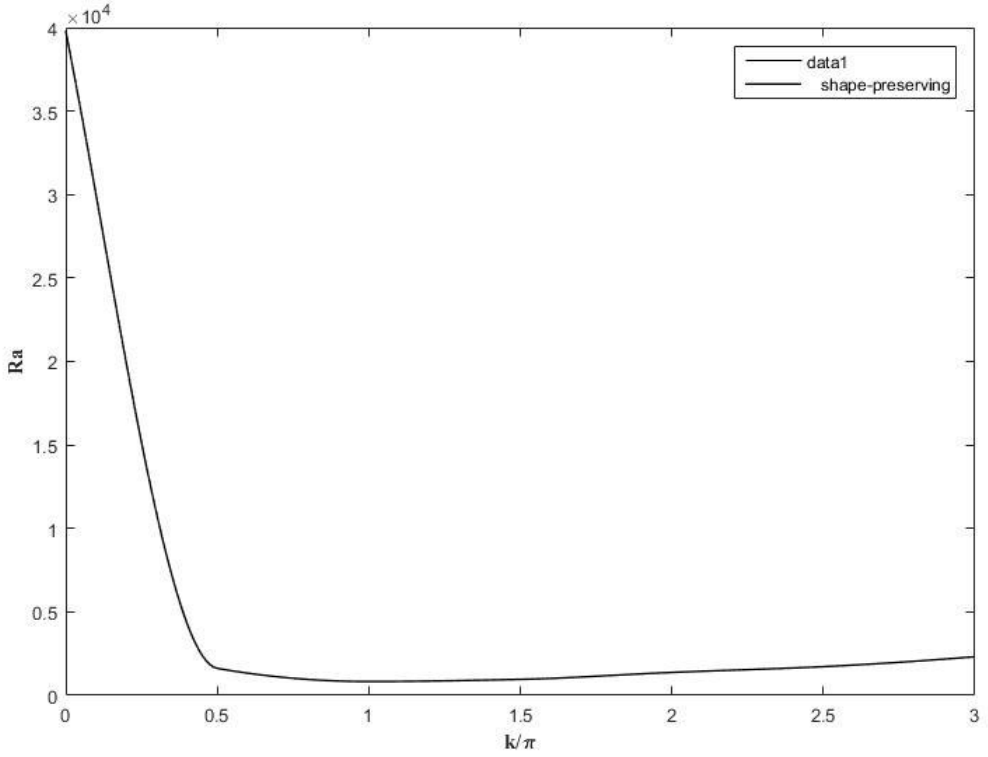

Figure 3.8: Critical Rayleigh number for different wave numbers

In most of the previous studies on the thermal convection of rarefied gases (Stefanov et al., 2002; Manela & Frankel, 2005), hard-sphere model was used. In the present analysis, we considered Maxwell model for deriving the transport coefficients. Though hard-sphere model has been popular because of its simplicity it fails to represent a realistic collision. In the hard-sphere model, interaction potential is assumed to be infinitely repelling only when the gas molecules are in contact with each other during a collision which is unrealistic because it is well known that the molecules tend to attract each other when they are apart for a finite distance. Though Maxwell model cannot address the attraction potential it predicts a diminishing repulsion potential as the molecules go apart from each other. The main advantage of Maxwell model lies in the fact that it can produce analytical expression just like the hard sphere model while addressing the molecular interaction more realistically.

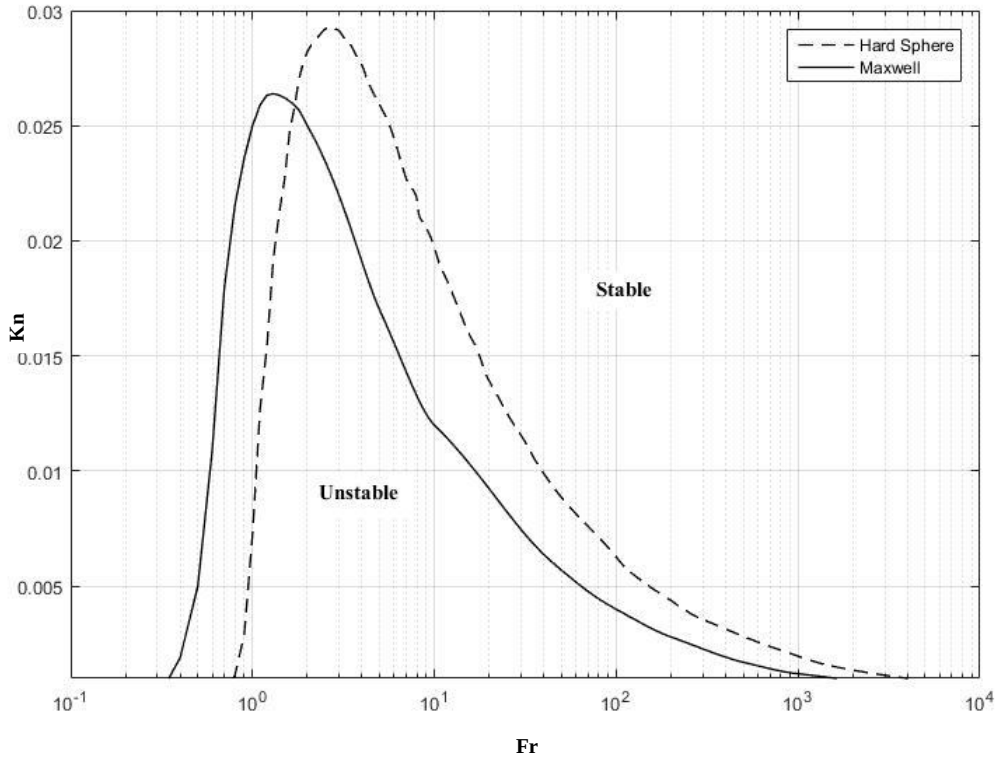

Figure 3.9: The neutral curves for two different gas models

The neutral curves over the (Fr, Kn) plane obtained using the Maxwell model and hard sphere model is shown in Figure 3.9. The results from Manela & Frankel (2005) have been used to reproduce the neutral curve for hard sphere model. When the system is fixed at a place, Fr is only affected by the temperature since the gap between two plates, D and gravitational constant, g are fixed. It is interesting to see that the curve obtained via Maxwell model shifts towards left; convection initiates at a lower temperature and the zone of convection is confined to lower temperature as well. This can be analyzed by looking at the transport coefficients for the two models. Both the models predict that the viscosity and thermal conductivity of the gas increase with temperature (Smirnov, 1982). Smirnov (1982) obtained the ratio of the transport coefficients for both hard sphere and Maxwell models. For a given temperature, hard sphere model predicts lower thermal conductivity and viscosity, approximately 94% of what Maxwell model predicts. On the right boundary of the neutral curves, it is not surprising that the unstable region is wider for hard sphere model than for the Maxwell model. This is because the viscosity which is

one of the causes for convection to be inhibited is predicted to be lower in the case of a hard sphere gas. However, on the left boundary, even though the viscosity for Maxwell model is higher than the hard sphere model convection can initiate early. This is because due to the presence of high compressibility effects at low Fr, the density distribution is not monotonically increasing from hot-bottom to cold-top plate following the relationship for an incompressible gas $\rho = \rho(T)$. Rather density is stratified in such a way that the gas is denser near the bottom plate. Under this circumstances, convection can still set in as discussed before but will initiate near the top cold plate. For such a localized convection to take place, the bottom surface still needs to be hot enough. Since the thermal conductivity of gases for Maxwell model is higher than the hard sphere model, heat from the bottom plate will conduct more effectively and will raise the temperature of the gas at an upper level higher. The critical temperature that is needed for a localized convection to set in near the top plate will be reached for the lower temperature of the bottom plate for Maxwell model.

3.3 Summary

The onset of convection in a rarefied gas cannot be determined by a single parameter like the Rayleigh number unlike the case of an incompressible fluid. The stability problem in a Rayleigh-Bénard configuration for rarefied gases is governed by the nondimensional temperature ratio, R_T, the Knudsen number and the Froude number. For the present analysis, a marginal stability curve in Kn-Fr plane has been obtained for $R_T = 0.1$. Convection sets in at any point inside the marginal stability curve while outside the curve there will always be pure conduction. The zone of convection is confined to Kn smaller than 0.026. The upper bound on Fr for the onset of convection is about 2000. Unlike the incompressible fluid, convection can start in a rarefied gas even when the density stratification is such that the fluid is denser near the bottom plate and lighter fluid rest upon them and the lower bound for Fr can be as low as 0.4 according to the present study. The comparison between the marginal stability curves obtained using two molecular interaction models, the hard-sphere and the Maxwell molecule, has been presented at the end of this chapter.

Chapter 4

4 Conclusions

Rayleigh-Bénard convection is one of the classical problems in hydrodynamic stability theory. A commonly accepted method to investigate this problem is to apply the Boussinesq approximation where the compressibility effects of are neglected. The transition to convection from a pure conduction state in a Raylegih-Bénard configuration is then determined by the Rayleigh number representing the relative effects of buoyancy, fluid viscosity, and heat conductivity. However, the necessary condition for the onset of convection is affected by the compressibility of the fluid which cannot be neglected in many cases including the large-scale convections in the atmosphere as well as the micro-nanoscale devices. In recent years, the investigation of the Rayleigh-Bénard problem in compressible fluids has attracted considerable attention. One of the popular approaches is to address this classical hydrodynamic stability problem for rarefied gases.

4.1 Summary

The onset of convection in rarefied gases in a Rayleigh-Bénard configuration has been analyzed. With the advancement of micro- nanoscale devices, rarefied gas phenomena have become important in many industrial applications such as electronic cooling, thermal actuators, vacuum packaging etc. One of the unique features of rarefied gas is that high-altitude conditions encountered in astrophysics including convection in stars and upper atmosphere of the Earth can be produced in a laboratory set-up with rarefied gas (Stefanov et al. 2002). Rayleigh-Bénard convection has been addressed for rarefied gases in recent years to model the compressible fluid problems. While DSMC has been a popular approach to solve the Rayleigh-Bénard problem for rarefied gases (Manela & Frankel 2005), continuum slip model has been used in this thesis. Unlike Manela who investigated the problem with a hard-sphere model, a more realistic Maxwellian model has been used to derive the state-dependent transport coefficients and the boundary conditions.

A linear stability analysis was conducted to mark the transition from conduction to convection in the Rayleigh-Bénard system with a rarefied gas. Before performing the linear stability analysis, a base state where pure conduction prevails was studied. The effects of Knudsen number, Froude number, and the accommodation coefficient have been shown in Chapter 2. As the Knudsen number increases, which is a measure of gas rarefaction, larger temperature-jump at the boundaries have been observed (Figure 2.1and 2.4). Because of higher rarefaction, the heat transfer rate decreases as Kn is increased (Figure 2.2 and 2.5). However, the density is only affected by the choice of Fr as can be seen from Figure 2.9. For large Fr, in the case of weak gravity, the density of the pure conduction state increases from the bottom-hot plate to top-cold plate. When strong gravity effects are present, for small Fr, the gas is stratified in such a way that the gas near the bottom plate is denser than those near the top plate even though the temperature of the bottom plate is higher. The density distribution is nonmonotonic for some intermediate values of Fr. The accommodation coefficient, χ affects the temperature-jump at the boundaries. A large fraction of molecules incident on the plates are thermalized, less temperature-jump is observed at the boundaries.

The stability of the pure conduction state has been examined by introducing small harmonic perturbations to the base state. After linearizing, the governing equations along with the boundary conditions for perturbations have been transformed into an algebraic eigenvalue problem using Chebyshev collocation method. A neutral curve has been obtained in the (Fr, Kn) plane for the critical wave number $k = \pi$ and temperature ratio $R_T = 0.1$ (Figure 3.1). Every point on the neutral curve marks the critical condition for the onset of convection while the zone outside the neutral curve represents the pure conduction state. Although a critical Rayleigh number indicates the onset of convection for incompressible fluids, the neutral curve in Figure 3.1 does not correspond to a single Rayleigh number since Ra depends on both Fr and Kn (3.11). For a given rarefaction (Kn), there can be two values of Fr that corresponds to the transition from the pure conduction to convection state. However, for each k there is a minimum Ra along the neutral curve which indicates the onset of convection. This minimum value of Ra has been recorded for different values of k (Figure 3.5). The lowest value of the minimum Ra

for different k corresponds to $k = \pi$ which has been found to be the critical wave number for compressible Rayleigh-Bénard convection by early authors, Jeng & Hassad, 1999 and Berbera, 2003. In the last section of Chapter 3, a comparison between the neutral curves obtained by the present study for a Maxwellian gas and by Manela for a hard-sphere gas has been presented. The shift of the neutral curve for a Maxwellian gas toward left, smaller Fr, can be understood from the different predictions transport coefficients in two models.

4.2 Key Findings

The onset of convection in a rarefied gas in a Rayleigh-Bénard configuration, unlike in the case for an incompressible fluid, cannot be determined by Rayleigh number only. In a rarefied gas problem, the density distribution does not follow a nonmonotonically increasing trend from the hot plate towards a cold plate. Due to compressibility effects, the density can be stratified in a way where the gas density is less at the cold plate than at the hot plate. As a result, the onset of convection must be determined using at least two non-dimensional parameters while keeping the third one constant. In the present analysis, the ratio of temperature differences between the plates were chosen as 0.1 and a netural curve was obtained which marks the transition to convection from a pure conduction state in terms of Froude and Knudsen numbers. Convection in rarefied gases can only be observed when the degree of rarefaction is less i.e. Kn is small. When the gas is highly rarefied (for Kn > 0.026), conduction state remains stable and no convection can set in. To account for the molecular interaction of gas particles, Maxwell's molecule was used which is more realistic than the hard-sphere model employed by previous researchers in studying the Rayleigh- Bénard convection in rarefied gases. The most critical wave number of the disturbances for the onset of convection was also examined and it was found to be 3.14 which is the same as the critical wave number for the case of an incompressible fluid.

4.3 Future Recommendation

The linear stability analysis can tell us whether the system is stable or unstable to infinitesimal disturbances but it cannot predict the ultimate flow that results from this instability. Linear stability analysis fails to determine the stability of the system for large disturbances which can be investigated using nonlinear stability analysis. While there have been a number of nonlinear stability analyses conducted by (Mareschal & Kestemont 1987; Given & Clementi 1989; Watanabe 2004) for within the framework of Boussinesq approximation, such an analysis needs to be done for rarefied gases.

A Maxwellian gas has been considered in this thesis to model the molecular interactions because it predicts the molecular repulsion in a more realistic way than the hard-sphere model. Yet, it is one of the simplest models which cannot represent the actual molecular interactions. Other models of molecular interaction should be explored to study the Rayleigh-Bénard problem in rarefied gases.

In this thesis, first order velocity-slip and temperature-jump boundary conditions have been applied. Boundary conditions with higher order slip discussed by Hadjiconstantinou (Manela & Frankel 2005) can be explored in the future. The neutral curve marking the onset of convection obtained in this thesis can also be reproduced for different boundary conditions such as constant and periodic heat flux applied to one or both plates. While the present study has focused only on a single value of temperature ratio, $R_T = 0.1$, other values of R_T needs to be examined in the future as well. The stability analysis for a Rayleigh-Bénard problem studied here could also be extended for other configurations such as double-layer fluids, vertical slots in window-panes.

Although the present study is not expected to predict the form and intensity of the final convection patterns which are governed by nonlinear interaction, this thesis successfully predicts the boundary of the convection domain. This offers the linear temporal stability analysis as a viable means of studying the how the various parameters affect the transition from the pure conduction state to convection in a rarefied gas.

References

AHLERS, G. 1980 Effect of departures from the Oberbeck-Boussinesq approximation on the heat transport of horizontal convecting fluid layers. *J. Fluid Mech.* 98, 137-148.

AHLERS, G., DRESSEL, B., OH, J., & PESCH, W. 2010 Strong non-Boussinesq effects near the onset of convection in a fluid near its critical point. *J. of Fluid Mech, 642*, 15-48.

ANISIMOV, M. A. 1991 *Critical Phenomena in Liquids and Liquid Crystals.* Gordon and Breach Science Publishers.

ASHKENAZI, S. & STEINBERG, V. 1993 Rayleigh-Bénard convection near the gas-liquid critical point. *Phys. Rev. Lett.* 70, 3888-3891.

BERGÉ, P. & DUBOIS, M. 1984 Rayleigh-Bénard convection. *Contemp. Phys.* 25, 6, 535-582.

BESKOK A., P. & KARNIADAKIS, G. E. & TRIMMER, W. 1996 Rarefaction and compressibility effects in gas microflows. *J. Fluids Eng.* 118, 448-456.

BESKOK A. 2001 Rarefied gas flows in microscale: Applications of RGD in MEMS. *AIP Conference Proceedings*. 585, 483.

BIRD, G. A. 1994 *Molecular Gas Dynamics and the Direct Simulation of Gas Flows*. Oxford University Press.

BOBYLEV, A. V. 2008 Generalized Burnett hydrodynamics. *J. Stat. Phys.* 132, 569.

BOBYLEV, A. V. & WINDFALL, A. 2012 Boltzmann equation and hydrodynamics at the Burnett level. *Kinet. Relat. Models. 5*, 237.

BODENSCHATZ, E., PESH, W. AND AHLERS, G., 2000, Recent developments in Rayleigh-Bénard convection, *Ann. Rev. Fluid Mech.*, 32, 709-778.

BORMANN, A. 2001 The onset of Rayleigh-Bénard problem for compressible fluids. *Continuum Mech. Thermodyn.* 13, 9-23.

BUSSE, F. H. 1967 The stability of finite amplitude cellular convection and its relation to an extremum principle Instabilities of convection rolls in a high Prandtl number fluid. *J. Fluid Mech.* 30, 625-649.

BUSSE, F. H. & WHITEHEAD, J. A. 1971 Instabilities of convection rolls in a high Prandtl number fluid. *J. Fluid Mech.* 47, 305-320.

CANUTO, C., HUSSAINI, M. Y., QUARTERONI, A. & ZANG, T. A. 2006 *Spectral Methods*. Spronger.

CERCIGNANI, C. 1975 *Theory and Application of the Boltzmann Equation*. Scottish Academic Press.

CERCIGNANI, C. 2000 *Rarefied Gas Dynamics*. Cambridge University Press.

CHANDRASEKHAR, S. 1961 *Hydrodynamic and Hydromagnetic Stability*. Clarendon.

CHAPMAN, S. & COWLING, T. G. 1970 *The Mathematical Theory of Non-Uniform Gases*. Cambridge University Press.

CHARRU, F. 2011 *Hydrodynamic Instabilities*. Cambridge University Press.

DRAZIN, P. G. & REID, W. H. 1981 *Hydrodynamic Stability*. Cambridge University Press.

DUAN, Z. & MUZYCHKA, Y. S. 2007 Slip Flow in non-circular microchannels. *Microfluidics and Nanofluidics.* 3, 473-484.

EMANUEL, K. A. 1994 *Atmospheric Convection*. Oxford University Press. FAN, J. & SHEN, C. 2001 Statistical simulation of low-speed rarefied gas flows. *J. Comput. Phys.* 167, 393.

FIELDING, S. M. 2008 Hydrodynamic Stability. Part I: Linear Staqbility Analysis. *Lecture notes, University of Manchester.*

FRÖLICH, J. LAURE, P. & PEYRET, R. 1992 Large departures from the Boussinesq approximation in the Rayleigh-Bénard problem. *Phys. Fluids.* 4, 1355-1372.

FURUKAWA, A., MEYER, H., ONUKI, A. & KOGAN, A. B. 2003 Convection in a very compressible fluid: Comparison of simulations with experiments. *Phys. Rev. E.* 68, 056309.

GARCIA, A. & PENLAND, C. 1991 Fluctuating hydrodynamics and principal oscillation pattern analysis. *J. Stat. Phys.* 64, 1121-1132.

GAUTHIER, S. & DOOLEN G. D. 1987 Compressible Rayleigh-Bénard spectral simulations: A useful reference solution. *Complex Systems.* 1, 727-734.

GOLSHTEIN, E. & ELPERIN, T. 1996 Convective instabilities in rarefied gases by direct simulation Monte Carlo method. *J. Thermophys. Heat Transfer.* 10, 250-256.

GITERMAN, M. 1978 C Hydrodynamics of fluids near a critical point. *Rev. Mod. Phys.* 50, 85, 325-331.

GETLING, A. V.1998 *Rayleigh-Bénard Convection; Structures and Dynamics.* World Scientific.

GHIAASIAAN, S. M. 2011 *Convective Heat and Mass Transfer*. Cambridge University Press.

GIVEN, J. A. & CLEMENTI, E. 1989 Molecular dynamics and Rayleigh-Bénard convection. *J. Chem. Phys.* 90, 7376.

GITERMAN, M. & SHTEINBERG, V. 1970 Criteria of occurrence of free convection in a compressible viscous heat-conducting fluid. *J. Appl. Maths Mech.* 34, 325-331.

GOTTLIEB, D., HUSSAINI, M. Y., ORSZAG, S. A. 1984 Theory and Applications of Spectral Methods. In: Voigt, R. G., Gottlieb, D., Hussaini, M. Y. (eds.): *Spectral Methods for Partial Differential Equations*. SIAM, Philadelphia.

GRAD, H. 1949 On the kinetic theory of rarefied gases. *Commun, Pure Appl. Math.* 2, 331.

GRAY, D. D. & GIORGINI, A. 1976 The validity of the Boussinesq approximation for liquids and gases. *Int. J. Heat Mass Trasfer.* 19, 545-551.

HADJICONSTANTINOU, N., GARCIA, A., BAZANT, M. & HE, G. 2003 Statistical error in particle simulation of hydrodynamic phenomena. *J. Comput. Phys.* 187, 274-297.

HAKEN, H. 1977 *Synergetics, An Introduction: Nonequilibrium Phase Transitions and Self-organization in Physics, Chemistry and Biology*. Springer.

HILLS, R. N. & ROBERTS, P. H. 1991 On the motion of a liquid that is incompressible in a generalized sense and its relationship to the Boussinesq approximation. *J. Stab. Appl. Anal. Cont. Media*. 1, 205-212.

HIRSCHFELDER, J. O., CURTISS, C. F. & BIRD, R. B. 1954 *Molecular Theory of Gases and Liquids*. John Wiley & Sons, Inc.

JEFFREYS, H. 1926 The stability of a layer of fluid heated below. *Phil. Mag.* 2, 833-844.

JEFFREYS, H. 1930 The instability of a compressible fluid heated below. *Math. Proc. Camb. Phil. Soc.* 26, 170-172.

JENG, J. & HASSARD, B. 1999 The critical wave number for the planar Bénard problem is unique. *Intl. J. Nonlinear Mech.* 34, 221-229.

KENNARD, E. H. 1938 *Kinetic Theory of Gases*. McGraw-Hill Book Company Inc.

KIERZENKA, J. & SHAMPINE, L. F. 2001 A BVP solver based on residual control and MATLAB PSE. *ACM Trans. Math. Softw.* 27, 299-316.

KOGAN, A. B. & MEYER, H. 2001 Heat transfer and convection onset in a compressible fluid: ^{3}He near the critical point. *Phys. Rev. E.* 63, 056310.

KOSCHMIEDER, E. 1993 *Bénard Celss and Taylor Vortices*. Cambridge University Press.

LANDAU, L. D. & LIFSHITZ, E.M. 1959 *Fluid Mechanics.* Pergamon.

LIU, H., WANG, M., WANG, J., ZHANG, G., LIAO, H., HUANG, R. & ZHANG, X. 2007 Monte Carlo simulations of gas flow and heat transfer in vacuum packaged MEMS devices. *Appl. Therm. Eng.* 27, 323-329.

MANELA, A. & FRANKEL, I. 2005 On the Rayleigh-Bénard problem in the continuum limit. *Phys. Fluids.* 17, 036101.

MARESCHAL, M. KESTEMONT, E. 1987 Experimental evidence for convective rolls in finite two-dimensional molecular models. *Nature.* 329, 427-429.

MAXWELL J.C. 1879 On stresses in rarefied gases arising from inequalities of temperature, *Phil. Trans. R. Soc. Lond.*, 170, 231-256.

MIHAHJA, J. M. 1962 A rigorous exposition of the Boussinesq approximations applicable to a thin layer fluid. *Astrophys. J.* 136, 1126-1133.

MULLER, I. 1985 *Thermodynamics.* Pitman Publishing.

MUTABAZI, I., WESFREID, J. E. & GUYON, E. 2006 *Dynamics of Spatio-Temporal Cellular Structures*. Springer.

NICOLIS, G. & PRIGOGINE, I. 1977 *Self-organization in Nonequilibrium Systems: From Dissipative Structures to Order Through Fluctuations*. Wiley.

NORMAND, C., POMEAU, Y. & VELARDE, M. 1977 Convective instability: A physicist`s approach. *Rev. Mod. Phys.* 49, 3, 581-624.

PAN, L. S., NG, T. Y., XU, D., LIU, G. R. & LAM, K. Y. 2002 Determination of temperature jump coefficient using the Direct Simulation Monte Carlo method. *J. Micromech. Microeng.* 12, 41-52.

PAOLUCCI, S. & CHENOWETH, D. R. 1987 Departures from the Boussinesq approximation in laminar Bénard convection. *Phys. Fluids.* 30, 1561-1564.

PELLEW, A. & SOUTHWELL, R. V. 1940 On maintained convective motion in a fluid heated from below. *Proc. R. Soc. Lond.* 176, 312-343.

PEREZ, C. R. & VELERDE M. G. 1975 On the non linear foundation of the Boussinesq approximation applicable to a thin layer of fluid. *J. Phys.* 36, 591-601.

PEYRET, R 2002 *Spectral Methods for Incompressible Viscous Flow*. Springer.

RAJAGOPAL, K. R., RUZICKA, M. & SRINIVASA, A. R. 1996 On Oberbeck-Boussinesq approximation. *Math. Models Meth. Appl. Sci.* 6, 8, 1157-1167.

RANA, A. S., TORRILHON, M., & STRUCHTRUP, H. 2013 A robust numerical method for the R13 equations of rarefied gas dynamics: Application to lid driven cavity. *J. Comput. Phys.* 236, 169.

RANA, A. S., MOHAMMADZADEH, A. & STRUCHTRUP, H. 2015 A numerical study of the heat transfer through a rarefied gas confined in a microcavity. *Continuum Mech. Thermodyn.* 27, 433-446.

RAYLEIGH, LORD. 1916 On convection currents in a horizontal layer of fluid, when the higher temperature is on the under side. *Phil. Mag.* 32, 539-546.

ROBINSON, F. & CHAN, K. 2004 Non-Boussinesq simulations of Rayleigh-Bénard convection in a perfect gas. *Phys. Fluids.* 16, 1321-1333.

ROBINSON, C. & HARVEY, J. 1997 Two -dimensional DSMC calculations of the Rayleigh-Bénard instability. In Rarefied Gas Dynamics 20. Edited by Shen, C. Peking University Press.

ROY, A. & STEINBERG, V. 2002 Reentrant hexagons in non-Boussinesq Rayleigh-Bénard convection: Effect of compressibility. *Phys. Rev. Lett.* 88, 244503.

SCHWARZSCHILD, K. & HÄRM, R. 1958 Evolution of very massive stars. *Astrophys. J.* 128, 348-360.

SCHUBERT, G., TURCOTTE, D. L. & OLSON, P. 2001 *Mantle Convection in the Earth and Planets*. Cambridge University Press.

SHU, J, TEO, J. B. M & CHAN, W. K. 2017 Fluid velocity slip and temperature jump at a solid surface. *Appl. Mech. Rev.* 69(2), 020801.

SMIRNOV, B. M. 1982 The hard-sphere model in plasma and gas physics. *Sov. Phys. Usp.* 25, 854-862.

SONE, Y., AOKI, K. & SUGIMOTO, H. 1997 The Bénard problem for a rarefied gas: Formation of steady flow patterns and stability of array of rolls. *Phys. Fluids.* 9, 3898-3914.

SOCHI, T. 2011 Slip at fluid-solid interface *Polymer Reviews.* 51, 309-340.

SPIEGEL, E. A. & VERONIS, G. 1960 On the Boussinesq approximation for a compressible fluid. *Astrophys. J.* 131, 442-447.

SPIEGEL, E. A. 1965 Convective instability in a compressible atmosphere. *Astrophys. J.* 141, 1068-1090.

STEFANOV, S. & CERCIGNANI, C. 1992 Monte Carlo simulation of Bénard`s instability in a rarefied gas. *Eur. J. Mech. B/Fluids.* 11, 543-554.

STEFANOV, S., ROUSSINOV, V. & CERCIGNANI, C. 2002 Rayleigh-Bénard flow of a rarefied gas and its attractors. I. Covection regime. *Phys. Fluids.* 14, 2255-2269.

STEFFEN, M., FREYTAG, B. & LUDWIG, H. G. 2005 3d simulation of convection and spectral line formation in a-type stars. In 13th Cambridge workshop on cool stars, stellar systems and the Sun, ESA Special Publication, 56, 985. Edited by Favata, F., Hussain, G. A. J. & Battrick, B.

STONE, H. A., STROOCK, A. D. & AJDARI, A. 2004 Engineering flows in small devices: Microfluidics towards lab-on-a-chip. *Annu. Rev. Fluid Mech.* 6, 381-411.

STRANGES, D. F., KHAYAT, R. E. & ALBAALBAKI, B. 2013 Thermal convection of non-Fourier fluids. *Intl. J. Thermal Sci.* 74, 14-23.

STRUCHTRUP, H. & WEISS, W. 2000 Temperature jump and velocity slip in the moment method. *Continuum Mech. Thermodyn.* 12, 1-8.

STRUCHTRUP, H. 2005 *Macroscopic Transport Equations for Rarefied Gas Flows*. Springer.

STRUCHTRUP, H. & TAHERI, P. 2011 Macroscopic transport models for rarefied gas flows: A brief review. *IMA J.. Appl. Math.* 76 (5), 672.

STRUCHTRUP, H. & TORRILHON, M. 2008 Boundary conditions for regularized 13-moment equations for micro-channel-flows. *J. Comput. Phys.* 227, 1981.

SU, Y. 1998 *Collocation spectral methods in the solution of Possion equation*. Retrieved from https://open.library.ubc.ca/cIRcle/collections/ubctheses/831/items/1.0080039.

SUGIMOTO, H., SONE, Y. AOKI, K. & MOTOHASHI, H. 1995 The Bénard problem of rarefied gas dynamics. In Rarefied Gas Dynamics 19. Edited by Harvey, J. & Lord, G. Oxford University Press.

WATANABE, T. 2004 Flow pattern and heat transfer in Rayleigh-Bénard convection. *Phys. Fluids.* 16, 972.

WATANABE, T., KABURAKI, H. & YOKOKAWA, M. 1994 Simulation of two-dimensional Rayleigh-Bénard system using the direct simulation Monte Carlo method. *Phys. Rev. E.* 49, 4060-4064.

TAHERI, P., TORRILHON, M. & STRUCHTRUP, H. 2009 Couette and Poiseuille microflows: Analytical solutions for regularized 13-moment equations. *Phys. Fluids.* 21, 017102.

TAHERI, P., RANA, A. S., TORRILHON, M. & STRUCHTRUP, H. 2009 macroscopic description of steady and unsteady rarefaction effects in boundary value problems of gas dynamics. *Contin. Mech. Thermodyn.*. 19, 273.

TRITTON, D. J. 1988 *Physical Fluid Dynamics*. Clarendon.

URBAN, P., HANZELKA, P., MUSILOVÁ, V., SRNKA, A. & SKRBEK, L. 2007 Design and tests of the cryostat with an experimental cell for turbulent thermal convection. *Proceedings of the Colloquium Fluid Dynamics*. Prague, the Czech Republic.

VARGAS, M., TATSIOS, G., VALOUGEORGIS, D. & STEFANOV, S. 2014 Rarefied gas flow in a rectangular enclosure induced by non-isothermal walls. *Phys. Fluids.* 26, 057101.

WAGNER, W. 1992 A convergence proof for Bird`s direct simulation Monte Carlo method for the Boltzmann equation. *J. Stat. Phys.* 66, 1011-1044.

YANG, H., WU, M. & FANG, W. 2005 Localized induction heating solder bonding for wafer level MEMS packaging. *J. Micromech. Microeng.* 15, 394-399.

ZAPPOLI, B., BEYSENS, D. & GARRABOS, Y. 2015 *T Heat Transfers and Related Effects in Supercritical Fluids.* Springer.

Appendix

Appendix A: Solving Boundary Value Problem by Chebyshev Collocation Method

Let us consider the following differential equation

$$u'' + xu' - u = \left(24 + 5x^2\right)e^{5x} + \left(2 + 2x^2\right)\cos\left(x^2\right) - \left(4x^2 + 1\right)\sin\left(x^2\right), \qquad \text{(A1)}$$

on $-1 \le x \le 1$

which we wish to solve.

The corresponding boundary conditions are

$$u(-1) = e^{-5} + \sin(1)$$

and $u(1) = e^5 + \sin(1)$.

The solution to the problem stated above is approximated by a polynomial $u_N(x)$ of degree at most equal to N. According to the collocation method, the differential equation (A1) is readily satisfied at the collocation points.

Let us take the Gauss-Lobatto collocation points

$$x_i = \cos\frac{\pi i}{k}, \quad i = 0, ..., k.$$

The differential equation in (A1) is forced to satisfy at the inner collocation points by an approximating polynomial $u_N(x)$. The collocation equation along with the boundary conditions are-

$$u_N''(x_i)+u_N'(x_i)-u_N(x_i)=f(x_i), \qquad i=1,....,N-1$$
$$u_N(x_N)=e^{-5}+\sin(1) \qquad \text{A2}$$
$$u_N(x_0)=e^{-5}+\sin(1)$$

where $f(x)=\left(24+5x^2\right)e^{5x}+\left(2+2x^2\right)\cos\left(x^2\right)-\left(4x^2+1\right)\sin\left(x^2\right)$, $g_-=e^{-5}+\sin(1)$, and $g_+=e^{5}+\sin(1)$.

Since the derivatives at any collocation points also need to be expressed in terms of $u_N(x)$, (A2) becomes-

$$\sum_{j=0}^{N} d_{i,j}^{(2)}u_N(x_j)+\sum_{j=0}^{N} d_{i,j}^{(1)}u_N(x_j)-u_N(x_i)=f(x_i), \qquad i=1,....,N-1$$
$$u_N(x_N)=g_-$$
$$u_N(x_0)=g_+$$

which a set of linear algebraic equations of the form $AU=F$.

Here $U=\left(u_N(x_0),u_N(x_1),...,u_N(x_{N-1}),u_N(x_N)\right)^T$, $F=\left(g_+,f_1,...,f_{N-1},g_-\right)^T$, and A is the $(N+1)x(N+1)$ matrix consisting of the differentiation coefficients, $d_{i,j}^{(2)}$ and $d_{i,j}^{(1)}$.

Figure A1.1. shows how the choice of number of collocation points affects the solution. The exact solution of the problem (A1) is hown by the solid line and two approximate solutions for N=5 and N=20 are indicated by dashed and dotted lines, respectively (Figure A1.1).

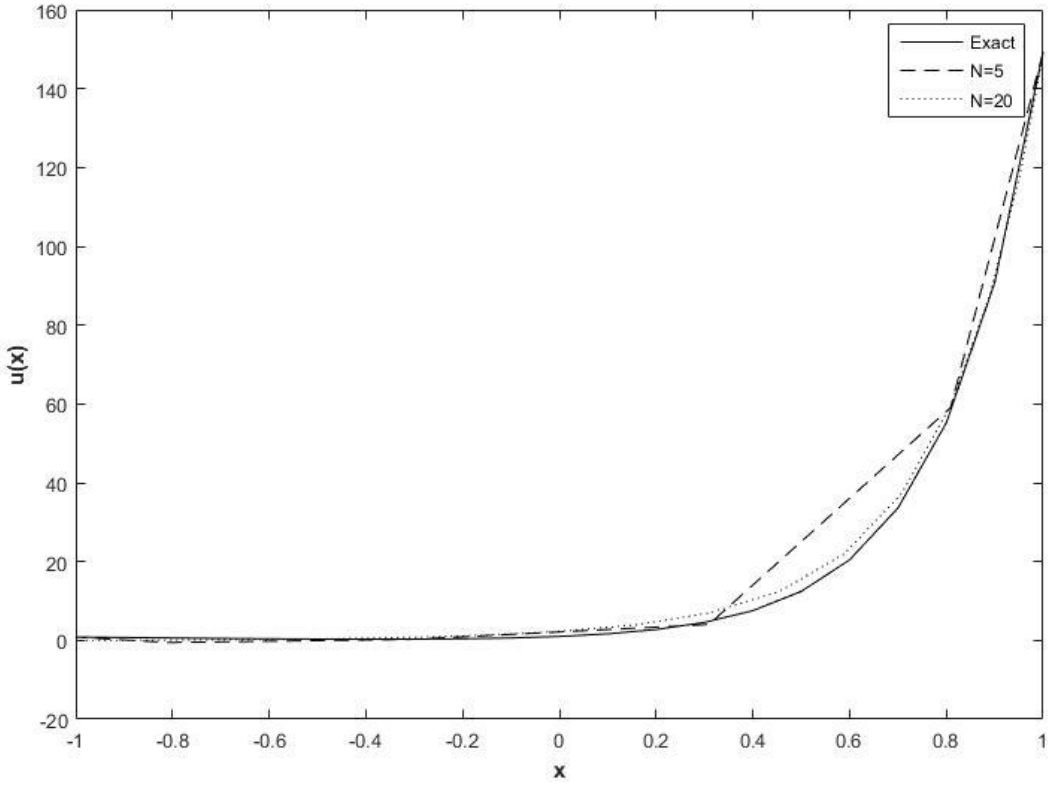

Figure A. 1: Effect of number of collocation points on a solution approximated with Chebyshev polynomial

Curriculum Vitae

Name:	Md Asif Zobaer
Post-secondary Education and Degrees:	Bangladesh University of Engineering and Technology Dhaka, Bangladesh 2008-2013 B.Sc. (Mechanical Engineering) The University of Western Ontario London, Ontario, Canada 2015-2017 (ongoing) M.E.Sc.
Honours and Awards:	Government of Bangladesh Technical Scholarship 2008-2012
Related Work Experience	Teaching Assistant The University of Western Ontario 2015-2017